Nonlinear Feedback Models of Hysteresis

JINHYOUNG OH, BOJANA DRINCIC, and DENNIS S. BERNSTEIN

BACKLASH, BIFURCATION, AND MULTISTABILITY

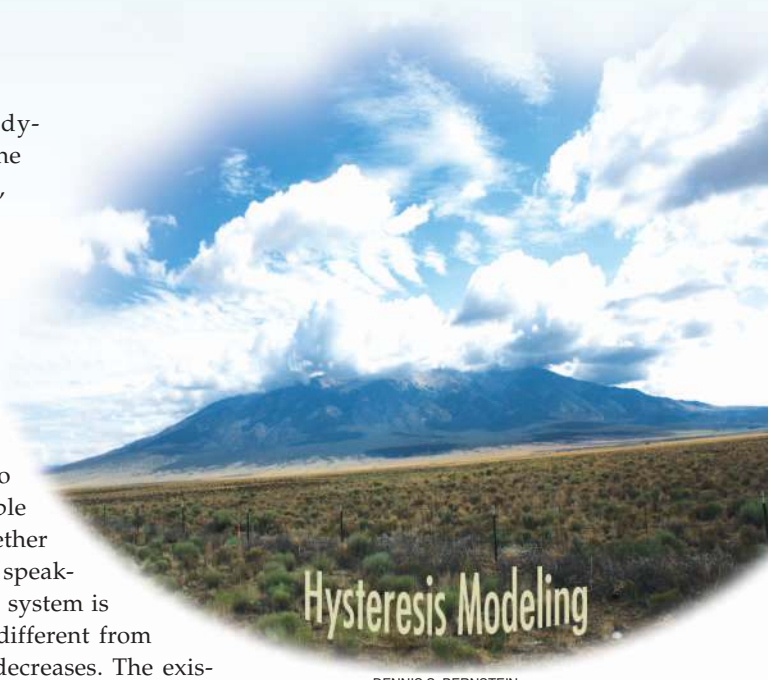

DENNIS S. BERNSTEIN

Hysteresis arises in diverse applications, including structural mechanics, aerodynamics, and electromagnetics [1]–[4]. The word "hysteresis" connotes lag, although this nomenclature is misleading since delay per se is not the mechanism that gives rise to hysteresis. As discussed in [5], hysteresis is a quasi-static phenomenon in which a sequence of periodic inputs produces a nontrivial input-output loop as the period of the input increases without bound. In this limit, the input can be viewed as completing its cycle increasingly slowly. This limiting input-output loop is due to the existence, for a given constant input, of multiple equilibria that map to distinct output values (whether or not the output map is one-to-one). Intuitively speaking, as the input slowly increases, the state of the system is attracted to input-dependent equilibria that are different from the attracting equilibria when the input slowly decreases. The existence of multiple attracting equilibria is called *multistability* [5]–[10]. Multistability corresponds to the intuitive notion that, under asymptotically slowly changing inputs, the state of a hysteretic system converges to equilibria that belong to an equilibrium set that has a multivalued structure, that is, multiple state equlibria can exist for a given constant input. To the extent that this phenomenon is history dependent, it is appropriate to say that a hysteretic system has memory.

For a single-input, single-output system, hysteresis is the persistence of a nondegenerate input-output closed curve as the frequency of excitation tends toward dc. Such systems are necessarily nonlinear since a linear system cannot have a nontrivial limiting closed input-output curve at asymptotically low frequencies. A hysteretic system whose periodic input-output map is the same for all frequencies is called *rate independent*; when the periodic input-output map is different for different frequencies, the hysteretic system is *rate dependent*. All of the hysteresis examples in this article exhibit rate-dependent hysteresis. The concept of rate-dependent hysteresis is thus central to the study of hysteresis arising in nonlinear feedback models.

Digital Object Identifier 10.1109/MCS.2008.930919

1066-033X/09/$25.00©2009IEEE

Various classes of models can give rise to hysteresis. The classical Preisach model [3] is given in terms of an integral whose kernel determines the shape of the hysteresis map; such models are rate independent. Alternatively, the finite-dimensional Duhem model [11]–[13] is modeled by an ordinary differential equation whose vector field depends on the derivative of the input. A Duhem model can exhibit either rate-independent or rate-dependent hysteresis. Yet another model of hysteresis is the nonlinear feedback model, in which a nonlinear feedback map gives rise to multiple attracting equilibria, the number of which varies as a function of the input [4, p. 17]. Examples show that hysteresis in nonlinear feedback models can arise from a wide variety of nonlinear functions, including saturation and deadzone.

In mechanical engineering applications, perhaps the most familiar example of hysteresis is backlash, which arises from free play in mechanical couplings. In practice, backlash often represents one of the main impediments to achievable performance, and efforts to model backlash and reduce its impact remain an active area of research [14]–[17]. Kinematic backlash can be modeled as the asymptotically low-frequency response of the feedback interconnection of linear dynamics and either a deadzone function or a stop or play nonlinearity [18], [19]. A related approach is given in [19].

A common feature of the Duhem and nonlinear feedback models is multistability, that is, the existence of multiple attracting equilibria [7]–[10]. The attracting equilibria may be isolated or they may constitute a continuum. In particular, the Duhem model has the property that, for every constant input, every state of the system is an equilibrium. In contrast, the nonlinear feedback model may have either a continuum of equilibria or isolated equilibria. We refer to hysteresis arising from a continuum of equilibria as *traversal-type hysteresis*, and hysteresis arising from isolated equilibria as *bifurcation-type hysteresis*. The latter type are related to relaxation oscillations; see [20, p. 69]. An equilibrium that is not isolated cannot be asymptotically stable, although it can be semistable. The semistable equilibria, which constitute a subset of the Lyapunov-stable equilibria, are those equilibria for which a trajectory beginning in a neighborhood converges to a Lyapunov stable equilibrium [21], [22].

In either case, that is, isolated or nonisolated equilibria, what is essential from the point of view of hysteresis is the fact that the trajectory converges for constant inputs. Step convergence refers to the convergence of trajectories to equilibria for all constant inputs. The relevance of step convergence to the existence of hysteresis lies in the fact that, in the dc limit, the system response depends on the convergence of the state for all constant inputs, that is, steps.

In the present article we investigate multistability and hysteresis within the context of linear systems with nonlinear feedback. For concreteness and simplicity, we focus primarily on single-input, single-output linear systems with companion-form realizations. For various choices of the realization parameters, we characterize the input-output equilibria set. We analyze this set in detail for the case of a deadzone nonlinearity, and we determine the values of the realization parameters that give rise to traversal-type or bifurcation-type hysteresis. The rich diversity of hysteretic phenomena that can be generated by interconnecting a linear system with a feedback nonlinearity is the motivation for this article.

The article is organized as follows. The following section introduces a nonlinear feedback model and defines the input-output equilibria set. Next, we define the limiting periodic input-output map, and we investigate the relationship between step convergence and the hysteresis maps of the nonlinear feedback model. We then discuss step convergence of the first-order nonlinear feedback model. Next, a nonlinear feedback model with deadzone is introduced, and its hysteresis maps are characterized. Finally, we give a multiloop nonlinear feedback example with two nonlinearities and discuss its hysteresis map.

NONLINEAR FEEDBACK MODEL

Consider the following single-input, single-output nonlinear feedback model

$$\dot{x}(t) = Ax(t) + Du(t) + By_\phi(t),$$
$$x(0) = x_0, \quad t \geq 0, \tag{1}$$
$$y(t) = Cx(t), \tag{2}$$
$$u_\phi(t) = E_1 x(t) + E_0 u(t), \tag{3}$$
$$y_\phi(t) = \phi(u_\phi(t)), \tag{4}$$

where $A \in \mathbb{R}^{n\times n}$, $D \in \mathbb{R}^n$, $B \in \mathbb{R}^n$, $C \in \mathbb{R}^{1\times n}$, $E_1 \in \mathbb{R}^{1\times n}$, $E_0 \in \mathbb{R}$, $u : [0, \infty) \to \mathbb{R}$ is continuous and piecewise C^1, $\phi : \mathbb{R} \to \mathbb{R}$ is a memoryless (static) nonlinearity, and $x(t), x_0 \in \mathbb{R}^n$. We assume that ϕ is globally Lipschitz, and thus the solution of (1)–(4) exists and is unique on all finite intervals. Under these assumptions, x and y are C^1. We also assume that (A, B, C) is minimal.

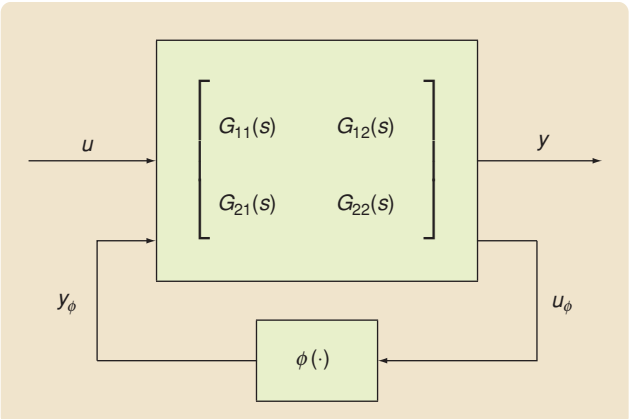

FIGURE 1 A feedback interconnection corresponding to the single-input, single-output system (1)–(4). The interconnection involves a two-input/two-output linear system and a feedback nonlinearity. Note that the model can be interpreted as the linear fractional transformation between the nonlinearity $\phi(\cdot)$ and G_{11}, G_{12}, G_{21}, and G_{22}.

Let $G_{11}(s) \triangleq C(sI_n - A)^{-1}D$, $G_{12}(s) \triangleq C(sI_n - A)^{-1}B$, $G_{21}(s) \triangleq E_1(sI_n - A)^{-1}D + E_0$, and $G_{22}(s) \triangleq E_1(sI_n - A)^{-1}B$. Then (1)–(4) can be interpreted as the linear fractional transformation between the nonlinearity $\phi(\cdot)$ and the transfer functions G_{11}, G_{12}, G_{21}, and G_{22}, which corresponds to the feedback interconnection of Figure 1.

The nonlinear feedback model (1)–(4) can be rewritten as

$$\dot{x}(t) = Ax(t) + D_1u(t) + B\phi(E_1x(t) + E_0u(t)), \tag{5}$$

$$y(t) = Cx(t), \qquad x(0) = x_0, \quad t \geq 0. \tag{6}$$

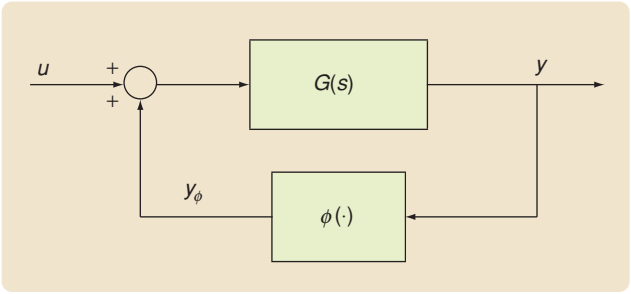

FIGURE 2 Feedback interconnection of the nonlinear hysteresis model (7), (8), where $G(s) \triangleq C(sI - A)^{-1}B$. This model is a simplification of the nonlinear feedback model in Figure 1 obtained by setting $D = B$, $E_0 = 0$, $E_1 = C$, that is, with $G_{11} = G_{12} = G_{21} = G_{22} = G(s)$.

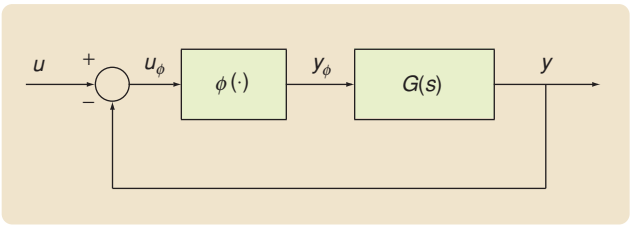

FIGURE 3 Feedback interconnection of the nonlinear feedback model (10), (11). This model is a simplification of the nonlinear feedback hysteresis model obtained by setting $D = 0$, $E_0 = 1$, and $E_1 = -C$, that is, with $G_{11} = 0$, $G_{12} = G(s)$, $G_{21} = 1$, and $G_{22} = -G(s)$.

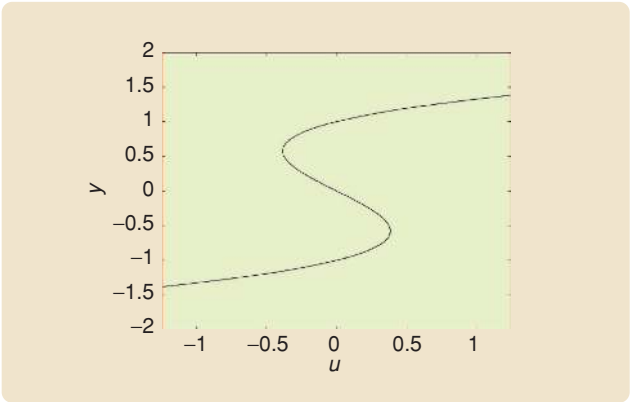

FIGURE 4 The input-output equilibria map $\mathcal{E}$ of (19) in Example 1. For all constant inputs $u(t) = \bar{u}$, the input-output equilibria map $\mathcal{E}$ is given by $\mathcal{E} = \{(\bar{u}, \bar{x}) \in \mathbb{R}^2 : -\bar{x}^3 + \bar{x} + \bar{u} = 0\}$.

Furthermore, let $D = B$, $E_0 = 0$, and $E_1 = C$. Then (5), (6) can be simplified as

$$\dot{x}(t) = Ax(t) + B(u(t) + \phi(y(t))), \tag{7}$$

$$y(t) = Cx(t), \qquad x(0) = x_0, \quad t \geq 0. \tag{8}$$

Figure 2 shows the feedback interconnection of (7), (8). Note that Figure 2 is a special case of Figure 1 with

$$\begin{bmatrix} G_{11}(s) & G_{12}(s) \\ G_{21}(s) & G_{22}(s) \end{bmatrix} = \begin{bmatrix} G(s) & G(s) \\ G(s) & G(s) \end{bmatrix}. \tag{9}$$

Alternatively, consider (5), (6) with $D = 0$, $E_0 = 1$, and $E_1 = -C$. Then an alternative specialization of (5), (6) is given by

$$\dot{x}(t) = Ax(t) + B\phi(u(t) - y(t)), \tag{10}$$

$$y(t) = Cx(t), \qquad x(0) = x_0, \quad t \geq 0. \tag{11}$$

Figure 3 shows the feedback interconnection of (10), (11). Note that Figure 3 is a special case of Figure 1 with

$$\begin{bmatrix} G_{11}(s) & G_{12}(s) \\ G_{21}(s) & G_{22}(s) \end{bmatrix} = \begin{bmatrix} 0 & G(s) \\ 1 & -G(s) \end{bmatrix}. \tag{12}$$

The equilibria of the simplified nonlinear feedback models (7), (8) and (10), (11) can be determined as follows. Since (A, B, C) is minimal, let A, B, and C be given in the controllable canonical form

$$A = \begin{bmatrix} 0 & 1 & \cdots & 0 \\ \vdots & \vdots & \ddots & \vdots \\ 0 & 0 & \cdots & 1 \\ -a_0 & -a_1 & \cdots & -a_{n-1} \end{bmatrix}, \quad B = \begin{bmatrix} 0 \\ \vdots \\ 0 \\ 1 \end{bmatrix},$$

$$C = [\, c_0 \quad c_1 \quad \cdots \quad c_{n-1} \,]. \tag{13}$$

Suppose $u(t) = \bar{u}$ is constant. Then the equilibrium $\bar{x}$ of (7) is given by

$$\bar{x} = [\, \bar{x}_1 \quad 0 \quad \cdots \quad 0 \,]^{\mathrm{T}}, \tag{14}$$

where $\bar{x}_1$ satisfies

$$a_0\bar{x}_1 = \phi(c_0\bar{x}_1) + \bar{u}. \tag{15}$$

Likewise, the equilibrium $\bar{x}$ of (10) is given by

$$\bar{x} = [\, \bar{x}_1 \quad 0 \quad \cdots \quad 0 \,]^{\mathrm{T}}, \tag{16}$$

where $\bar{x}_1$ satisfies

$$a_0\bar{x}_1 = \phi(\bar{u} - c_0\bar{x}_1). \tag{17}$$

Note that the equilibria of (7) and (10) are determined only by a_0 and c_0. The following definition is useful.

Definition

The input-output equilibria map $\mathcal{E}$ of (5), (6) is the set of points $(\bar{u}, C\bar{x}) \in \mathbb{R}^2$ such that $\bar{u}$ and $\bar{x}$ satisfy

$$A\bar{x} + D_1\bar{u} + B\phi(E_1\bar{x} + E_0\bar{u}) = 0. \tag{18}$$

The input-output equilibria map $\mathcal{E}$ is a possibly multivalued map between $\bar{u} \in \mathbb{R}$ and the corresponding equilibria of (5) as determined by (6). Since (18) is equivalent to (14) and (15) when (7), (8) hold, or to (16), (17) when (10), (11) hold, it follows that the input-output equilibria map $\mathcal{E}$ of either (7), (8) or (10), (11) can be characterized by analyzing (15) or (17). Note that $\mathcal{E}$ for the simplified nonlinear feedback models (7), (8) and (10), (11) is determined by the parameters a_0 and c_0.

Example 1

Consider the cubic model [23, p. 30]

$$\dot{x}(t) = -x^3(t) + x(t) + u(t), \qquad x(0) = x_0, \quad t \geq 0, \tag{19}$$

which is equivalent to (7), (8) with $A = B = C = 1$ and $\phi(v) = -v^3$. The equilibria of (19) with constant $u(t) = \bar{u}$ is given by (14), (15) with $a_0 = -1$ and $c_0 = 1$. Thus the input-output equilibria map $\mathcal{E}$ of (19) is given by $\mathcal{E} = \{(\bar{u}, \bar{x}) \in \mathbb{R}^2 : -\bar{x}^3 + \bar{x} + \bar{u} = 0\}$, which is shown in Figure 4.

Example 2

Consider the mass/dashpot/spring with gap model shown in figures 5 and 6 and modeled by

$$\begin{aligned} m\ddot{x}(t) + c\dot{x}(t) + kd_{2w}(x(t) - u(t)) &= 0, \\ x(0) = x_0, \quad t \geq 0, \end{aligned} \tag{20}$$

which is equivalent to (10) and (11) with

$$A = \begin{bmatrix} 0 & 1 \\ 0 & -\frac{c}{m} \end{bmatrix}, \quad B = \begin{bmatrix} 0 \\ \frac{k}{m} \end{bmatrix}, \quad C = \begin{bmatrix} 1 & 0 \end{bmatrix}, \tag{21}$$

where

$$d_{2w}(v) \triangleq \begin{cases} v - w, & v > w, \\ 0, & |v| \leq w, \\ v + w, & v < -w. \end{cases} \tag{22}$$

The equilibria of (20) with constant $u(t) = \bar{u}$ is given by (16), (17) with $a_0 = 0$ and $c_0 = 1$. Thus the input-output equilibria map $\mathcal{E}$ of (20) is given by $\mathcal{E} = \{(u, y) \in \mathbb{R}^2 : u - w \leq y \leq u + w, \ u \in \mathbb{R}\}$, which is shown in Figure 7.

Now, setting $A = 0$, $B = k/m$, and $C = 1$ yields the single integrator with deadzone model [24]

$$m\dot{x}(t) + kd_{2w}\Big(x(t) - u(t)\Big) = 0. \tag{23}$$

The equilibria of (23) with constant $u(t) = \bar{u}$ is also given by (16), (17) with $a_0 = 0$ and $c_0 = 1$, and thus $\mathcal{E} = \{(u, y) \in \mathbb{R}^2 : u - w \leq y \leq u + w, \ u \in \mathbb{R}\}$. Figure 7 shows the input-output equilibria map $\mathcal{E}$ of (23). Note that $\mathcal{E}$ of (20) and $\mathcal{E}$ of (23) are identical, since a_0 and c_0 are the same for both models.

HYSTERETIC MAPS OF NONLINEAR FEEDBACK MODELS

In this section we consider the step-convergent nonlinear feedback model (5), (6). The following definitions from [25] are needed.

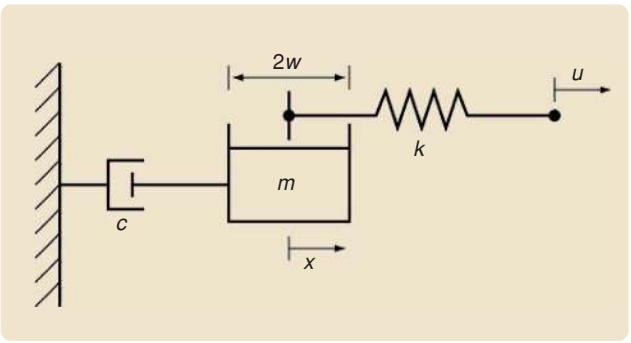

FIGURE 5 Mass-dashpot-spring system with deadzone. The input u is the position of the end of the spring, while the output x is the position of the mass.

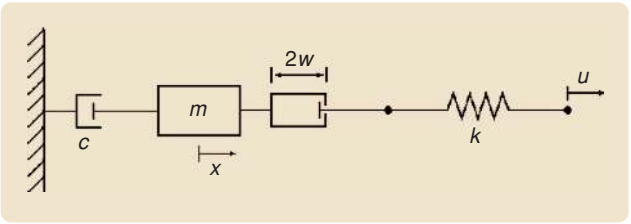

FIGURE 6 Equivalent representation of the mass-dashpot-spring system with deadzone shown in Figure 5. The symbolic representation of the deadzone corresponds to the play operator discussed in [19].

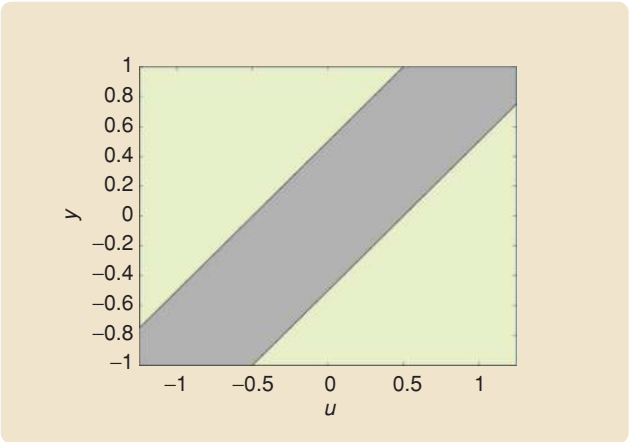

FIGURE 7 The input-output equilibria map $\mathcal{E}$ of (20) and (23) in Example 2 with $w = 0.5$. Note that $\mathcal{E}$ corresponding to (20) and $\mathcal{E}$ corresponding to (23) are identical.

The word "hysteresis" connotes lag, although this nomenclature is misleading since delay per se is not the mechanism that gives rise to hysteresis.

Definition

Consider (5) with constant $u(t) = \bar{u}$. The system (5) is *step convergent* if $\lim_{t\to\infty} x(t)$ exists for all $x_0 \in \mathbb{R}^n$ and for all $\bar{u} \in \mathbb{R}$.

Definition

The nonempty set $\mathcal{H} \subset \mathbb{R}^2$ is a *closed curve* if there exists a continuous, piecewise C^1, and periodic map $\gamma : [0, \infty) \to \mathbb{R}^2$ such that $\gamma([0, \infty)) = \mathcal{H}$.

Definition

Let $u : [0, \infty) \to [u_{\min}, u_{\max}]$ be continuous, piecewise C^1, periodic with period α and have exactly one local maximum $u_{\max}$ in $[0, \alpha)$ and exactly one local minimum $u_{\min}$ in $[0, \alpha)$. For all $T > 0$, define $u_T(t) \triangleq u(\alpha t/T)$, assume that there exists $x_T : [0, \infty) \to \mathbb{R}^n$ that is periodic with period T and satisfies (5) with $u = u_T$, and let $y_T : [0, \infty) \to \mathbb{R}$ be given by (6) with $x = x_T$ and $u = u_T$. For all $T > 0$, the *periodic input-output map* $\mathcal{H}(u_T, x_T(0))$ is the closed curve $\mathcal{H}(u_T, x_T(0)) \triangleq \{(u_T(t), y_T(t)) : t \in [0, \infty)\}$, and the *limiting periodic input-output map* $\mathcal{H}_\infty(u, x_0)$, where $x_0 \triangleq \lim_{T\to\infty} x_T(0)$, is the closed curve $\mathcal{H}_\infty(u, x_0) \triangleq \lim_{T\to\infty} \mathcal{H}(u_T, x_T(0))$ if the limit exists. If there exist $(u, y_1), (u, y_2) \in \mathcal{H}_\infty(u, x_0)$ such that $y_1 \neq y_2$, then $\mathcal{H}_\infty(u, x_0)$ is a *hysteretic limiting periodic input-output map* or a *hysteresis map*, and the system is *hysteretic*.

Note that the existence of $\lim_{T\to\infty} \mathcal{H}(u_T, x_T(0))$ refers to the convergence of the sets $\mathcal{H}(u_T, x_T(0))$ in the Hausdorff norm [12].

Suppose (5) is step convergent. Then it follows from the above definitions that $\lim_{t\to\infty} x(t)$ exists for every constant $u(t) = \bar{u}$ and is an equilibrium of (5). Now, let $u(t) \in [u_{\min}, u_{\max}]$ be periodic with period α. Let $u_T(t) = u(\alpha t/T)$, and suppose the *periodic input-output map* $\mathcal{H}(u_T, x_0)$ exists for all $T > 0$. Furthermore, assume the *limiting periodic input-output map* $\mathcal{H}_\infty(u, x_0)$ exists. The above definitions suggest that there exists a close relationship between $\mathcal{H}_\infty(u, x_0)$ and the input-output equilibria map $\mathcal{E}$ of (5), (6). The set $\mathcal{H}_\infty(u, x_0)$ represents the response of the system in the limit of dc operation, that is, as $T \to \infty$ and thus as $\omega = (2\pi/T) \to 0$, that is, dc. Therefore, each element of $\mathcal{H}_\infty(u, x_0)$ is the limit of a sequence of points in $\mathcal{H}(u_T, x_T(0))$ for an increasing, unbounded sequence of values of T, that is, for a sequence of increasingly slower inputs. Consequently, the limiting point $(\bar{u}, \bar{y}) \in \mathcal{H}_\infty(u, x_0)$ arises from an equilibrium under the constant input $u(t) = \bar{u}$. This observation indicates that the step convergence of (5), (6) is a necessary condition for the existence of $\mathcal{H}_\infty(u, x_0)$.

However, not every point in $\mathcal{H}_\infty(u, x_0)$ is in $\mathcal{E}$. If (5), (6) has a bifurcation, that is, a change in the qualitative structure of the equilibria as u changes, then the limiting solution of (5), (6), which is not C^1, can alternate between the components of $\mathcal{E}$. In this particular case, the limiting periodic input-output map $\mathcal{H}_\infty(u, x_0)$ contains vertical components that connect subsets as illustrated in Example 4. With the exception of the vertical segments that connect components of $\mathcal{E}$, it turns out that $\mathcal{H}_\infty(u, x_0) \subseteq \mathcal{E}$.

The relationship between $\mathcal{H}_\infty(u, x_0)$ and $\mathcal{E}$ elucidates the mechanism of hysteresis in the nonlinear feedback model. Since the definition of hysteresis requires that the hysteretic limiting periodic input-output map have at least two distinct points (u, y_1) and (u, y_2), a necessary condition for (5), (6) to be hysteretic is that $\mathcal{E}$ be a multivalued map. However, not every nonlinear feedback model that has a multivalued map $\mathcal{E}$ exhibits hysteresis since $\mathcal{H}_\infty(u, x_0) \subseteq \mathcal{E}$ can still be a single-valued map as illustrated in Example 3. The nonlinear feedback models that exhibit hysteresis have either a multivalued map $\mathcal{E}$ with a continuum of equilibria or a bifurcation for some $u \in [u_{\min}, u_{\max}]$ as demonstrated by the following numerical examples.

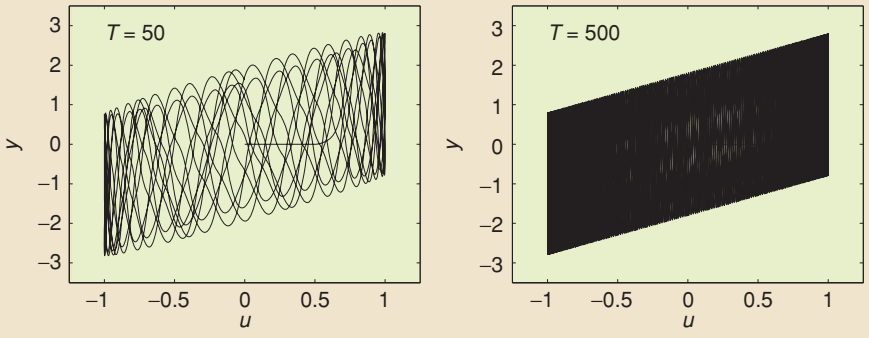

FIGURE 8 Input-output equilibria maps of Example 3 with $u_T(t) = \sin(2\pi/T)t$. Note that the model is not step convergent, and thus $\mathcal{H}_\infty(u, x_0)$ does not exist.

Example 3

Consider (10), (11) with

$$A = \begin{bmatrix} 0 & 1 \\ 0 & 2 \end{bmatrix}, \quad B = \begin{bmatrix} 0 \\ 1 \end{bmatrix}, \quad C = \begin{bmatrix} 2 & 3 \end{bmatrix},$$

and $\phi(v) = d_{2w}(v)$, where $w = 0.5$. The step response with $u(t) = 0.5$ and $x_0 = [1 \quad 2]^{\mathrm{T}}$ is bounded but does not converge. Hence, this system is not step convergent. Figure 8 shows the input-output map with $u_T(t) = \sin(2\pi/T)t$. Since the model is not step convergent, $\mathcal{H}_\infty(u, x_0)$ does not exist.

Example 4

Reconsider the cubic model (19) in Example 1 with $u_T(t) = \sin(2\pi/T)t$. Figure 9 shows that $\mathcal{H}(u_T, x_T(0))$ converges to a hysteretic limiting periodic input-output map as $T \to \infty$, and thus (19) is hysteretic.

Now, let $u(t) = \bar{u}$ be a constant. Since $(\mathrm{d}/\mathrm{d}x)(-x^3 + x + \bar{u}) = -3x^2 + 1$, linearization shows that, for each $\bar{u} \in (-(2/3\sqrt{3}), (2/3\sqrt{3}))$, the corresponding equilibrium $\bar{x} \in (-(1/\sqrt{3}), (1/\sqrt{3}))$ is unstable, whereas $\bar{x} \in (-\infty, -(1/\sqrt{3}))$ is asymptotically stable for all $|\bar{u}| > (2/3\sqrt{3})$. Therefore, as shown in Figure 10, $\mathcal{E}$ consists of points that arise either from asymptotically stable equilibria or from unstable equilibria.

Note that (19) has bifurcations at $\bar{u} = -(2/3\sqrt{3})$ and $\bar{u} = (2/3\sqrt{3})$. When $|\bar{u}| < (2/3\sqrt{3})$, (19) has two asymptotically stable equilibria and one unstable equilibrium, thus $\mathcal{E}$ is a multivalued map. On the other hand, when $|\bar{u}| \geq (2/3\sqrt{3})$, (19) has only one asymptotically stable equilibrium, and thus $\mathcal{E}$ is a single-valued map. Suppose u_T is pointwise approaching the dc limit of operation and $|u_T| < (2/3\sqrt{3})$ such that the solution of (19) converges to one of the asymptotically stable equilibria. Now, suppose u_T changes and a bifurcation occurs. Then (19) loses one of its asymptotically stable equilibria and the solution is attracted to another asymptotically stable equilibrium, generating a transition trajectory from the multivalued map to the single-valued map in $\mathcal{H}(u_T, x_T(0))$. The transition trajectories are represented by the vertical lines in Figure 10. Consequently, the limiting points in $\mathcal{H}_\infty(u, x_0)$ comprise a subset of $\mathcal{E}$ as well as vertical components at the bifurcation points, as shown in Figure 10. Note, however, that the vertical components in

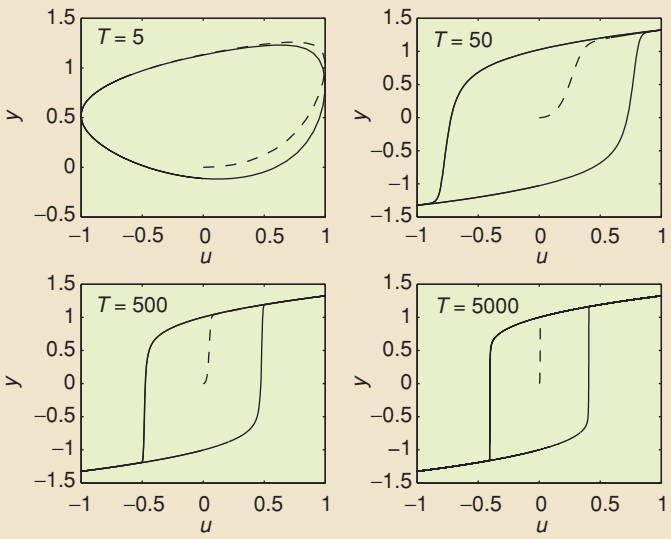

FIGURE 9 Periodic input-output map $\mathcal{H}(u_T, x_T(0))$ for the cubic model in Example 4 with $u_T(t) = \sin(2\pi/T)t$ for several values of T. For each value of T, the transient approach to the periodic input-output map is shown. The system is step convergent, and $\mathcal{H}(u_T, x_T(0))$ converges to a hysteretic limiting periodic input-output map $\mathcal{H}_\infty(u_T, x_0)$ as $T \to \infty$, and thus the system is hysteretic.

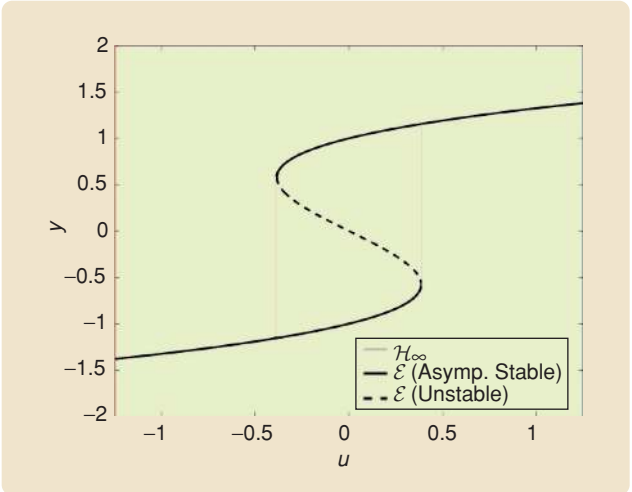

FIGURE 10 The input-output equilibria set $\mathcal{E}$ and the limiting periodic input-output map $\mathcal{H}_\infty(u, x_0)$ of the cubic model in Example 4. $\mathcal{E}$ consists of points arising from asymptotically stable (solid) equilibria and from unstable (dashed) equilibria. Note that $\mathcal{H}_\infty(u, x_0) \subseteq \mathcal{E}$ except for the vertical limiting transition trajectories between subsets of $\mathcal{E}$.

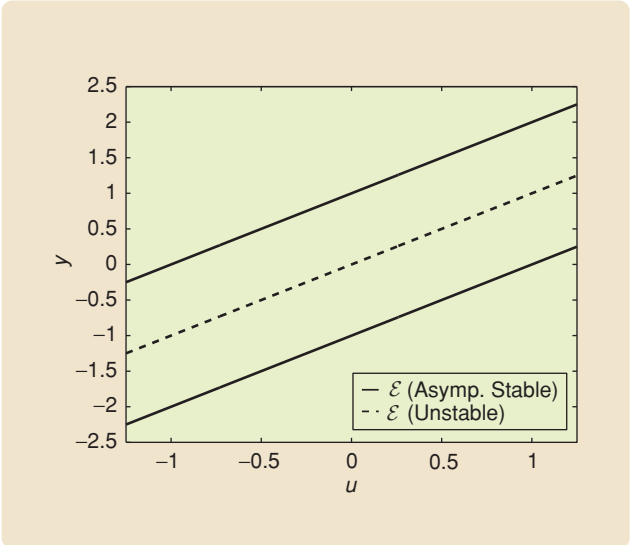

FIGURE 11 The input-output equilibria map $\mathcal{E}$ of (24) in Example 5. $\mathcal{E}$ consists of points arising from asymptotically stable (solid) equilibria and from unstable (dashed) equilibria.

$\mathcal{H}_\infty(u, x_0)$ are limits of subsets of trajectories (u_T, y_T) as $T \to \infty$.

Example 5

Consider the nonlinear system

$$\dot{x}(t) = (u(t) - x(t))^3 - (u(t) - x(t)),$$
$$x(0) = x_0, \quad t \geq 0, \tag{24}$$

which can be written as (10), (11) with $A = 0$, $B = 1$, $C = 1$, and $\phi(v) = v^3 - v$. The set of equilibria $\bar{x}$ of (24) with constant $u(t) = \bar{u}$ are given by $\{\bar{u}, \bar{u} - 1, \bar{u} + 1\}$. Since $(\mathrm{d}/\mathrm{d}x)[(\bar{u} - x)^3 - (\bar{u} - x)] = -3(\bar{u} - x)^2 + 1$, linearization shows that $\bar{x} = \bar{u}$ is an unstable equilibrium, and $\bar{x} = \bar{u} - 1$ and $\bar{x} = \bar{u} + 1$ are asymptotically stable equilibria. Therefore, $\mathcal{E} = \{(u, u - 1) : u \in \mathbb{R}\} \cup \{(u, u) : u \in \mathbb{R}\} \cup \{(u, u + 1) : u \in \mathbb{R}\}$ as shown in Figure 11.

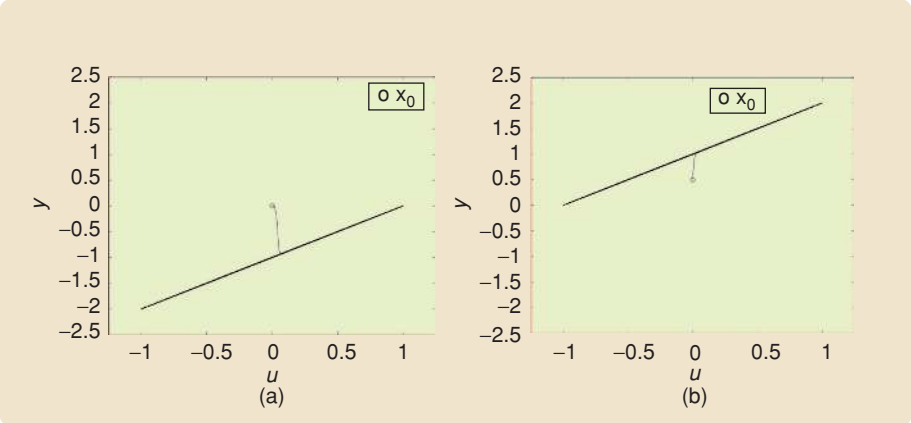

FIGURE 12 The periodic input-output maps of (24) in Example 5 with $u(t) = \sin 0.01t$ where (a) $x_0 = 0$ and (b) $x_0 = 0.5$. Note that (24) is not hysteretic although $\mathcal{E}$ of (24) is a multivalued map as shown in Figure 11.

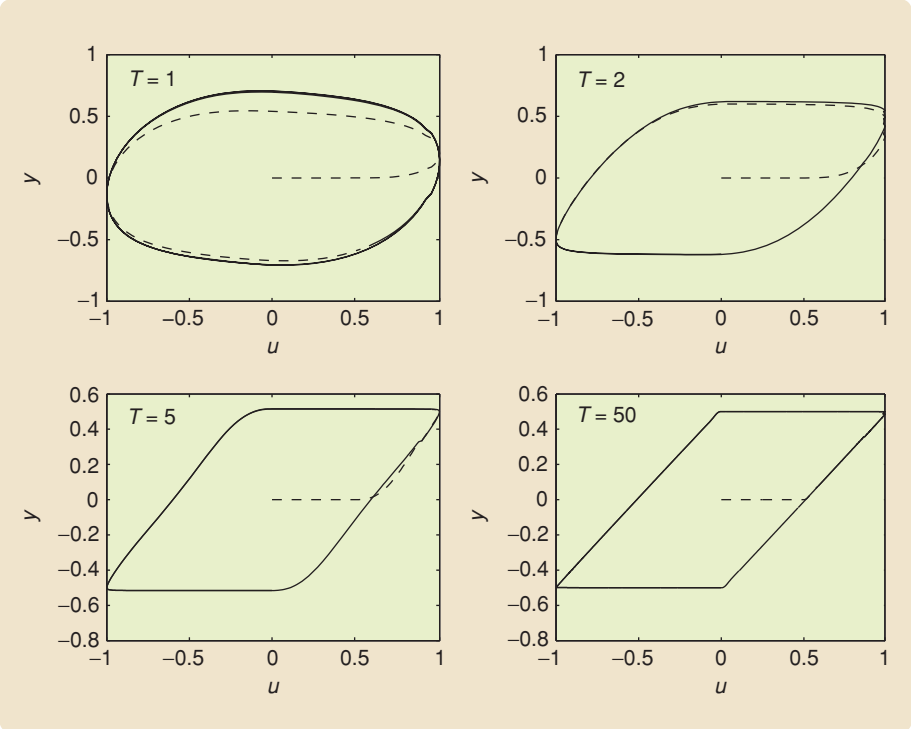

FIGURE 13 Periodic input-output map for the mass-dashpot-spring system with a deadzone shown in Figure 5, where $w = 0.5$, $m = 0.1$, $k = 10$, $c = 1$, and $u_T(t) = \sin(2\pi/T)t$ for several values of T. For each value of T, the transient approach to the periodic input-output map is shown. This system exhibits rate-dependent hysteresis because the periodic input-output maps for varying values of T are not identical. The hysteresis map in the lower right is the classical backlash.

Figure 12(a) and (b) show the periodic input-output maps of (24) with different initial conditions. Note that, although $\mathcal{E}$ is a multivalued map, the input-output map collapses to a single-valued map in both cases, indicating that (24) is not hysteretic.

Example 6

Reconsider the mass/dashpot/spring with gap model (20) with $u_T(t) = \sin(2\pi/T)t$. Figure 13 shows that $\mathcal{H}(u_T, x_T(0))$ converges to a hysteretic limiting input-output map, and thus (20) is hysteretic. Note that $\mathcal{E}$ consists of points arising from a continuum of input-dependent equilibria. Suppose u_T is sufficiently slow and the solution of (20) converges to an equilibrium in the equilibria continuum, and thus (u_T, y_T) is in the interior of $\mathcal{E}$. When u_T changes, the solution remains in the continuum of equilibria and thus y_T is constant. Therefore, (u_T, y_T) transverses horizontally in the interior of $\mathcal{E}$ until it reaches the boundary. Now, when (u_T, y_T) leaves the boundary of $\mathcal{E}$, the solution converges back to the boundary of the set of continua, and (u_T, y_T) follows the boundary of $\mathcal{E}$ as u_T changes. Consequently, the limiting input-output map $\mathcal{H}_\infty(u, x_0)$ of (20) consists of two horizontal components and parts of the boundary of $\mathcal{E}$ as shown in Figure 14.

Example 7

Consider the nonlinear system

$$\dot{x}(t) = -x(t) + \frac{w}{2}\sin \eta x(t) + u(t), \tag{25}$$

where $\eta > 0$, for $t \geq 0$ with $x(0) = 0$, which can be rewritten as (7), (8) with $A = -1$, $B = C = 1$, and $\phi(v) = (w/2)\sin \eta v$. Figure 15 shows $\mathcal{E}$ of (25) for several values of η. Note that $\mathcal{E}$ of (25) converges to $\mathcal{E}$ of (20) in Figure 14 as $\eta \to \infty$. Figure 16 shows $\mathcal{H}_\infty(u, x_0)$ with varying values of η. Note that $\mathcal{H}_\infty(u, x_0)$ for this example converges to $\mathcal{H}_\infty(u, x_0)$ of (20) as $\eta \to \infty$.

GRAPHICAL ANALYSIS OF NONLINEAR FEEDBACK MODELS

In this section we consider the step convergence for a first-order nonlinear feedback model by analyzing the phase portrait of the model. Specifically, consider (5) with constant $u(t) = \bar{u}$, and let $A,\ D,\ B,\ E_1,\ E_0 \in \mathbb{R}$. Since (5) is a first-order ordinary differential equation, the sign of the right-hand side of (5) determines the direction of the solution x. If $Ax_0 + D\bar{u} + B\phi(E_1x_0 + E_0\bar{u}) < 0$, x is decreasing and converges either to an equilibrium or to $-\infty$ as $t \to \infty$. Similarly, if $Ax_0 + D\bar{u} + B\phi(E_1x_0 + E_0\bar{u}) > 0$, x is increasing and converges either to an equilibrium or to ∞ as $t \to \infty$. Therefore, we can construct the phase portrait of (5) from the graph of the right-hand side of (5) for all $\bar{u} \in \mathbb{R}$ and determine the step convergence of the model.

To illustrate this graphical analysis, consider the cubic model (19) with constant $u(t) = \bar{u}$. Suppose $\bar{u} = 0$. Then the solution of (19) converges to one of its equilibria as shown in the phase portrait in Figure 17(a).

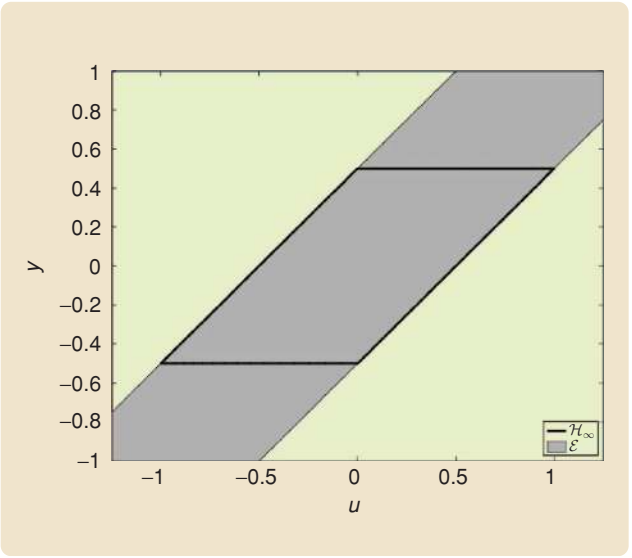

FIGURE 14 The input-output equilibria map $\mathcal{E}$ and the limiting periodic input-output map $\mathcal{H}_\infty(u, x_0)$ of the mass/dashpot/spring with deadzone model in Example 6. $\mathcal{H}_\infty(u, x_0)$ consists of two horizontal components and parts of the boundary of $\mathcal{E}$.

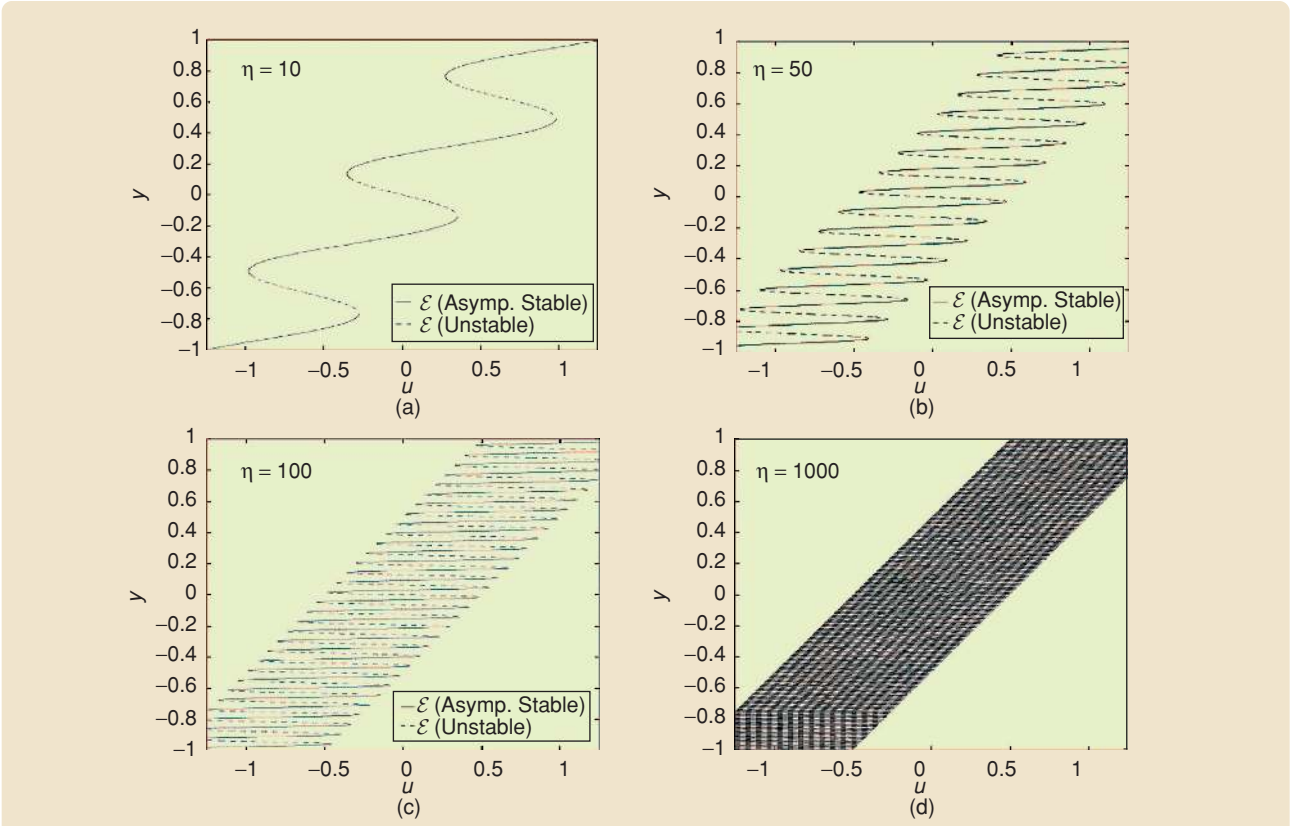

FIGURE 15 The input-output equilibria map $\mathcal{E}$ corresponding to (25) in Example 7 with (a) $\eta = 10$, (b) $\eta = 50$, (c) $\eta = 100$, and (d) $\eta = 1000$. Note that $\mathcal{E}$ corresponding to (25) converges to $\mathcal{E}$ corresponding to (20) in Figure 14 as $\eta \to \infty$.

For a single-input, single-output system, hysteresis is the persistence of a nondegenerate input-output closed curve as the frequency of excitation tends toward dc.

When $-(1/\sqrt{3}) < \bar{u} < (1/\sqrt{3})$, the qualitative structure of the phase portrait does not change. For $\bar{u} = -(1/\sqrt{3})$ or $\bar{u} = (1/\sqrt{3})$, (19) loses one of its asymptotically stable equilibria, and a bifurcation occurs. However, as shown in the phase portraits in Figure 17(b) and (c), the solution still converges to one of the equilibria. For $|\bar{u}| > (1/\sqrt{3})$, (19) has only one asymptotically stable equilibrium, and thus the solution converges to the equilibrium globally. This phase portrait analysis shows that the solution of (19) converges to an equilibrium point for all $x_0 \in \mathbb{R}$ and for all $\bar{u} \in \mathbb{R}$, and therefore (19) is step convergent.

Example 8

Consider the nonlinear system

$$\dot{x}(t) = -x(t) + u(t) + \tan^{-1} 2x(t),$$
$$x(0) = x_0, \quad t \geq 0, \tag{26}$$

which can be written as (7), (8) with $A = -1$, $B = 1$, $C = 2$, and $\phi(v) = \tan^{-1} v$. Figure 18 shows the phase portraits of (26) with several constants $u(t) = \bar{u}$. For $-(\pi - 2/4) < \bar{u} < (\pi - 2/4)$, (26) has two asymptotically stable equilibria and the solution converges to one of the equilibria as shown in Figure 18(a).

For $\bar{u} = -(\pi - 2/4)$ or $\bar{u} = (\pi - 2/4)$, a bifurcation occurs, and (26) loses one of its asymptotically stable equilibria, yet its solution still converges to one of the equilibria as shown in Figure 18(b) and (c). For $|\bar{u}| > (\pi - 2/4)$, (26) is globally asymptotically stable as shown in Figure

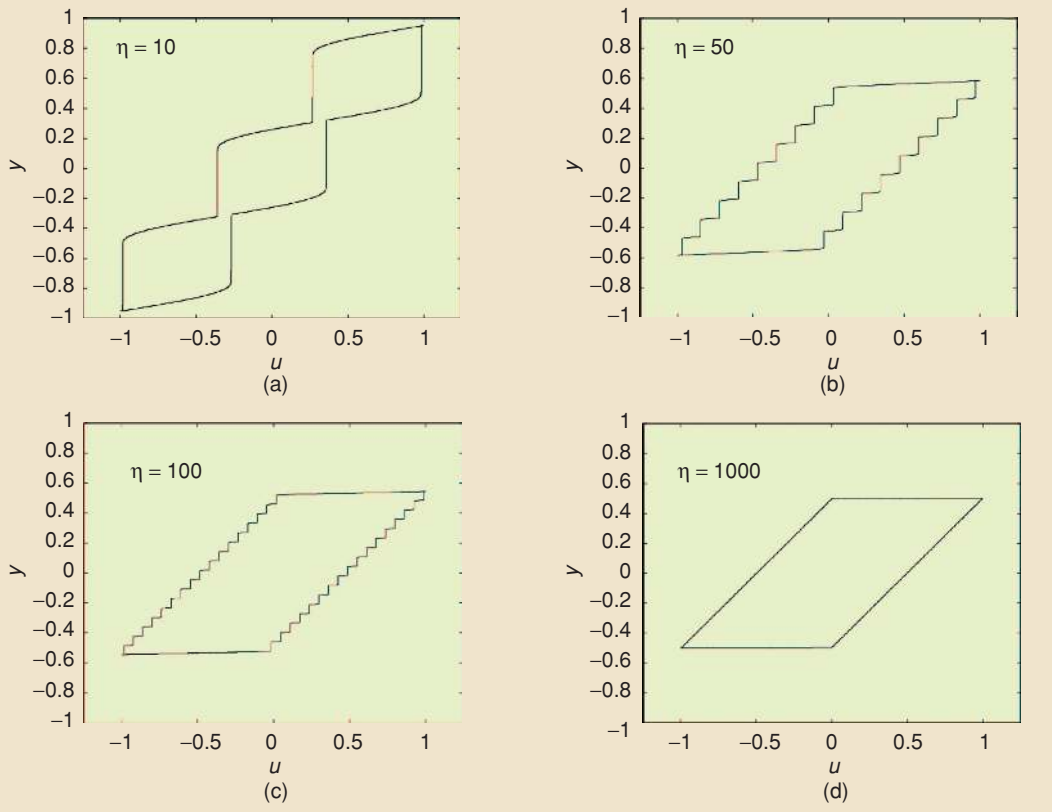

FIGURE 16 The limiting periodic input-output map $\mathcal{H}_\infty(u, x_0)$ corresponding to (25) in Example 7 with (a) $\eta = 10$, (b) $\eta = 50$, (c) $\eta = 100$, and (d) $\eta = 1000$. Note that $\mathcal{H}_\infty(u, x_0)$ corresponding (25) converges to $\mathcal{H}_\infty(u, x_0)$ corresponding to (20) in Figure 14 as $\eta \to \infty$.

18(d). Therefore, (26) is step convergent. Figure 19 shows that $\mathcal{H}(u_T, x_T(0))$ converges to a hysteretic map as $T \to \infty$.

Example 9

Consider the nonlinear system

$$\dot{x}(t) = -x(t) + \mathrm{sat}_w(u(t) + 2x(t)),$$
$$x(0) = x_0, \quad t \geq 0, \tag{27}$$

where

$$\mathrm{sat}_w(v) \triangleq \begin{cases} w, & v > w, \\ v, & |v| \leq w, \\ -w, & v < -w, \end{cases}$$

which can be written as (10), (11) with $A = -1$, $B = 1$, $C = -2$, and $\phi(v) = \mathrm{sat}_w(v)$. Figure 20 shows the phase portraits of (27) with various constants $u(t) = \bar{u}$. For $-(1/2) < \bar{u} < (1/2)$, (27) has two asymptotically stable equilibria, and the solution converges to one of the equilibria as shown in Figure 20(a).

For $\bar{u} = -(1/2)$ or $\bar{u} = (1/2)$, a bifurcation occurs, and (27) loses one of its asymptotically stable equilibria, yet its solution still converges to one of the equilibria as shown in Figure 20(b) and (c). For $|\bar{u}| > (1/2)$, (27) is globally asymptotically stable as shown in Figure 20(d). Therefore,

The concept of rate-dependent hysteresis is central to the study of hysteresis arising in nonlinear feedback models.

(27) is step convergent. Figure 21 shows that $\mathcal{H}(u_T, x_T(0))$ converges to a hysteresis map as $T \to \infty$.

Example 10

Consider the nonlinear system

$$\dot{x}(t) = x(t) + u(t) - d_{2w}(2x(t)), \quad x(0) = x_0, \quad t \geq 0, \tag{28}$$

which can be written as (7), (8) with $A = 1$, $B = 1$, $C = -2$, and $\phi(v) = d_{2w}(v)$. Figure 22 shows the phase portraits of (28) with several constants $u(t) = \bar{u}$. For $-(1/4) < \bar{u} < (1/4)$, (28) has two asymptotically stable equilibria, and the solution converges to one of the equilibria as shown in Figure 22(a).

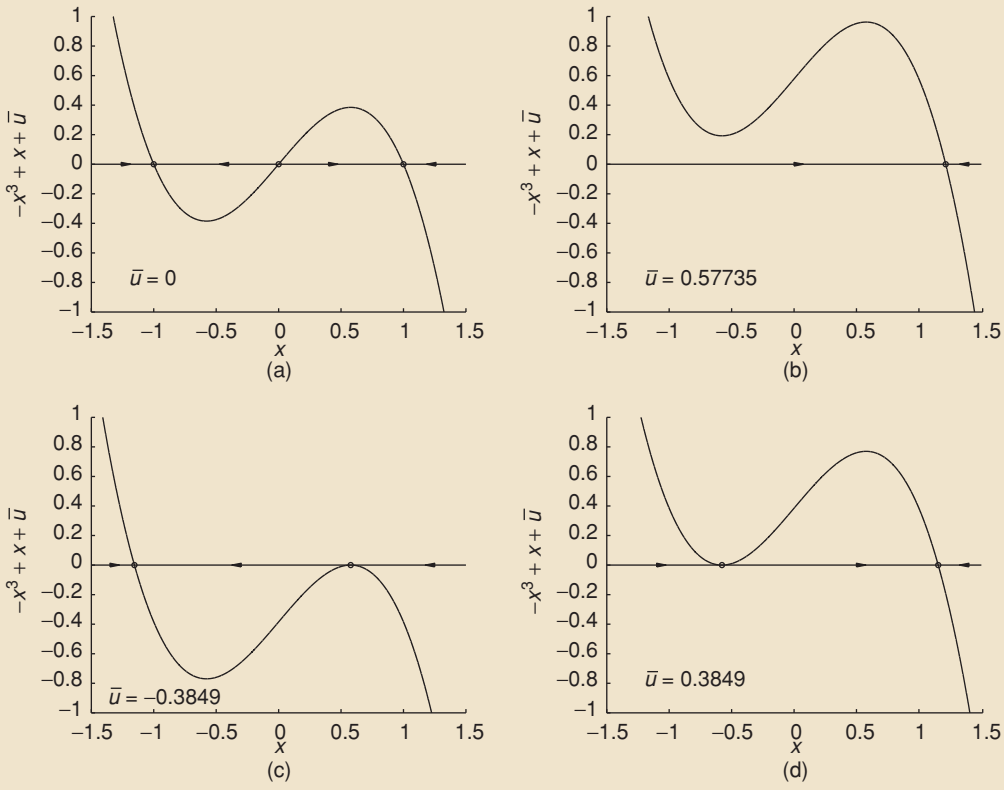

FIGURE 17 Plots of $-x^3 + x + \bar{u}$ and the phase portraits of (19), where (a) $\bar{u} = 0$, (b) $\bar{u} = -(2/3\sqrt{3})$, (c) $\bar{u} = (2/3\sqrt{3})$, and (d) $\bar{u} = (1/\sqrt{3})$. The phase portrait analysis shows that (19) is step convergent.

We refer to hysteresis arising from a continuum of equilibria as traversal-type hysteresis, and hysteresis arising from isolated equilibria as bifurcation-type hysteresis.

For $\bar{u} = -(1/4)$ or $\bar{u} = (1/4)$, a bifurcation occurs, and (28) loses one of its asymptotically stable equilibria, yet its solution still converges to one of the equilibria as shown in Figure 22(b) and (c). For $|\bar{u}| > (1/4)$, (28) is globally asymptotically stable as shown in Figure 22(d). Therefore, (28) is step convergent. Figure 23 shows that $\mathcal{H}(u_T, x_T(0))$ converges to a hysteresis map as $T \to \infty$.

NONLINEAR FEEDBACK MODELS WITH DEADZONE

As a specialization of (10) and (11), we consider the *nonlinear feedback model with deadzone*

$$\dot{x}(t) = Ax(t) + Bd_{2w}(u(t) - y(t)), \tag{29}$$

$$y(t) = Cx(t), \qquad x(0) = x_0, \quad t \geq 0, \tag{30}$$

where $A \in \mathbb{R}^{n\times n}$, $B \in \mathbb{R}^n$, $C \in \mathbb{R}^{1\times n}$, $u : [0, \infty) \to \mathbb{R}$ is continuous and piecewise C^1, and $d_{2w} : \mathbb{R} \to \mathbb{R}$ is a deadzone function with width $2w$ given by

$$d_{2w}(v) \triangleq \begin{cases} v - w, & v > w, \\ 0, & |v| \leq w, \\ v + w, & v < -w. \end{cases} \tag{31}$$

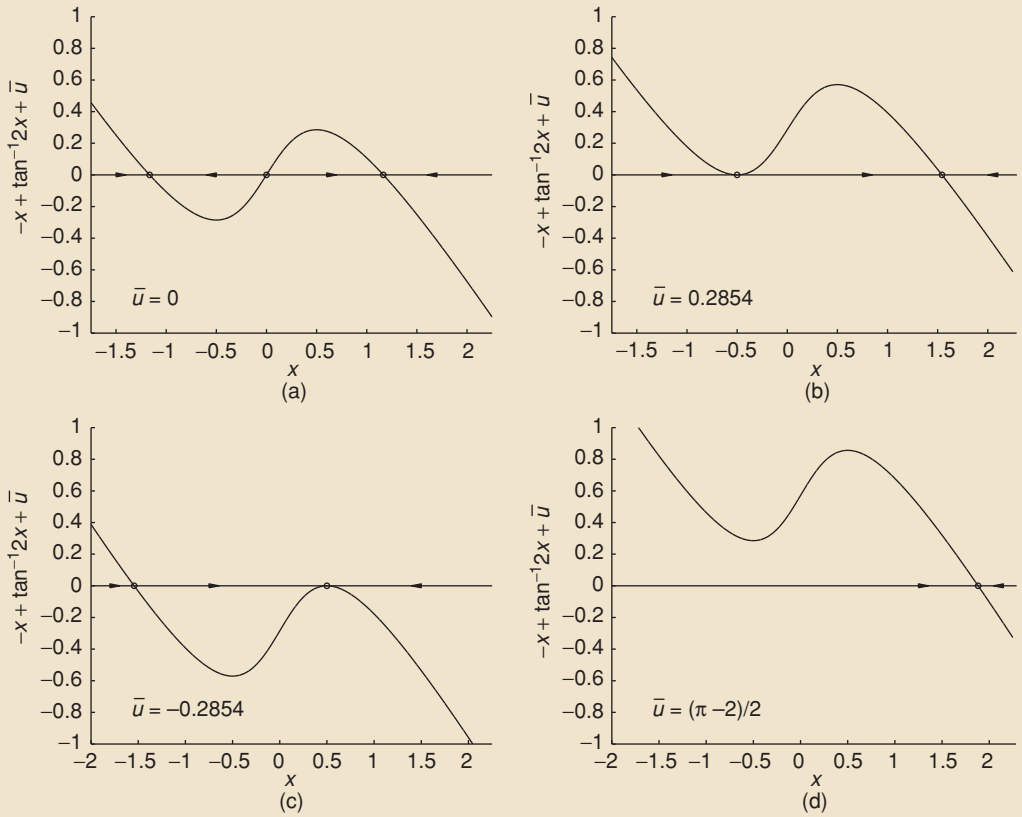

FIGURE 18 Plots of $-x + \bar{u} + \tan^{-1} 2x$ and the phase portraits of (26) in Example 8, where (a) $\bar{u} = 0$, (b) $\bar{u} = (\pi - 2)/4$, (c) $\bar{u} = -(\pi - 2)/4$, and (d) $\bar{u} = (\pi - 2)/2$. The phase portrait analysis shows that (26) is step convergent.

The equilibrium $\bar{x}$ of (29) is given from (16) and (17) by

$$\bar{x} = [\,\bar{x}_1 \quad 0 \quad \cdots \quad 0\,]^{\mathrm{T}}, \qquad (32)$$

where $\bar{x}_1$ satisfies

$$a_0\bar{x}_1 + d_{2w}(c_0\bar{x}_1 - \bar{u}) = 0. \qquad (33)$$

By determining the solutions of (32), (33), we can characterize the limiting equilibria map $\mathcal{E}$ of (29), (30) by the following cases. Note that $\mathcal{E}$ is nonempty since, for all $\bar{u} \in [-w, w]$, $\bar{x}_1 = 0$ satisfies (33), and thus $\{(\bar{u}, 0) : \bar{u} \in [-w, w]\} \subseteq \mathcal{E}$.

Case 1

Let $a_0 \neq 0$ and $a_0 + c_0 = 0$. Then, as shown in Figure 24, (33) has four types of solutions depending on the value of $\bar{u}$, namely, a continuum of solutions $\mathcal{X} = \{\bar{x} \in \mathbb{R} : (\operatorname{sign} c_0)\bar{x} \geq 0\}$ for $\bar{u} = -w$, a unique solution

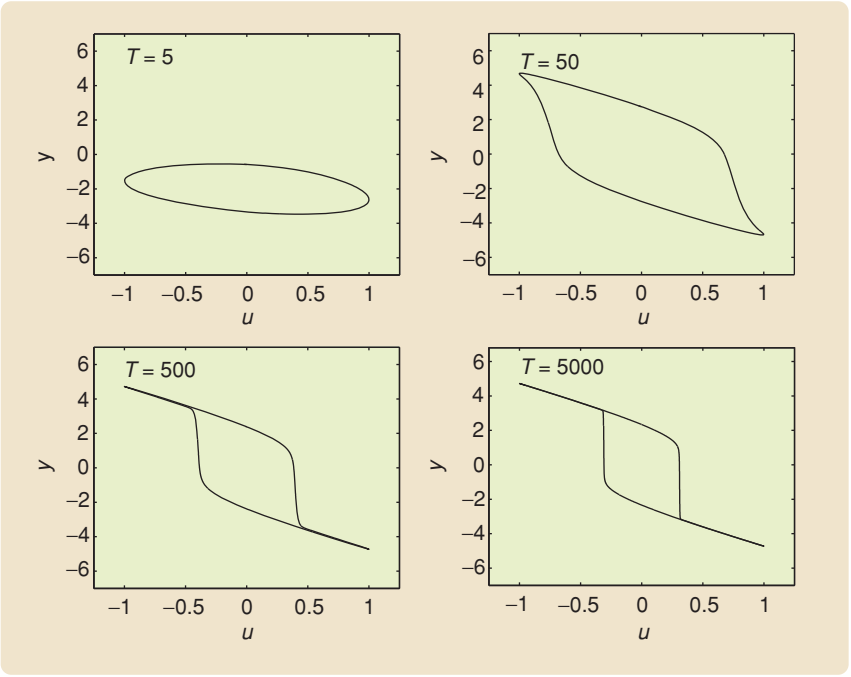

FIGURE 19 Hysteresis arising from the arctangent nonlinearity. This periodic input-output map $\mathcal{H}(u_T, x_T(0))$ corresponds to (26) in Example 8 with $u_T(t) = \sin(2\pi/T)t$. Note that $\mathcal{H}(u_T, x_T(0))$ converges to a hysteretic map $\mathcal{H}_\infty(u, x_0)$.

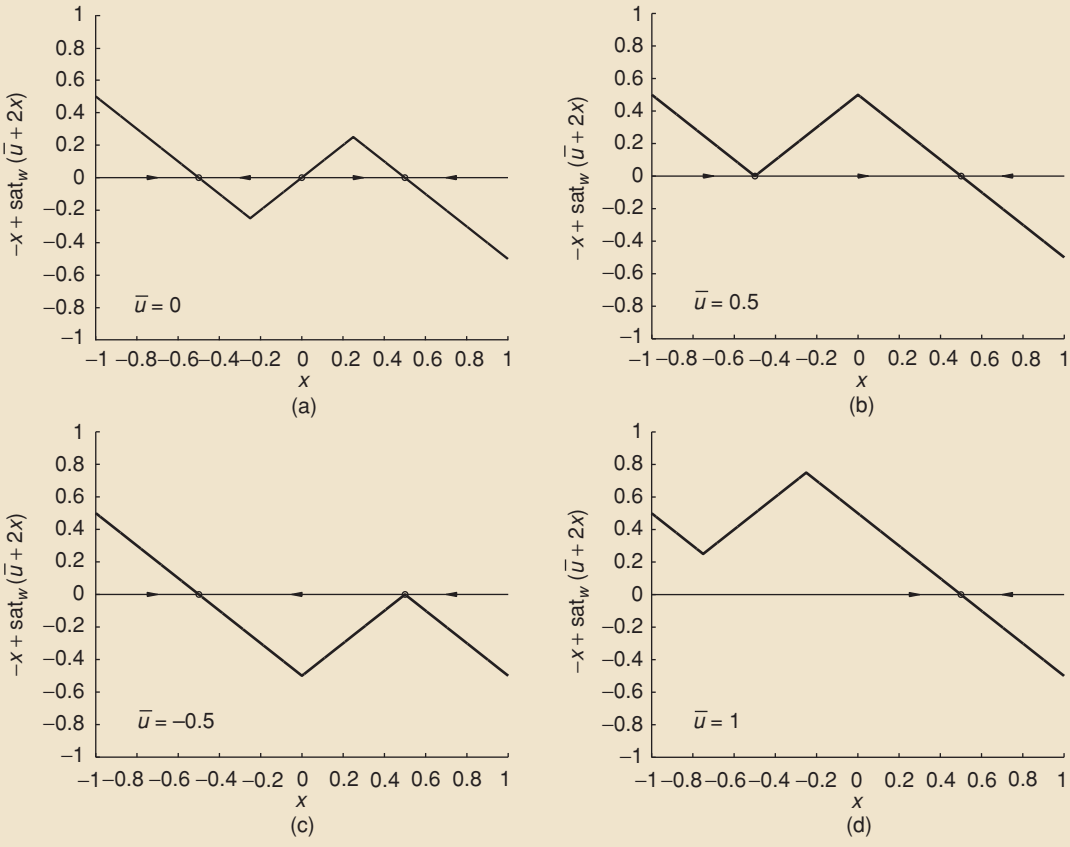

FIGURE 20 Plots of $-x + \mathrm{sat}_w(\bar{u} + 2x)$ and the scalar phase portraits of (27) in Example 9, where (a) $\bar{u} = 0$, (b) $\bar{u} = 1/2$, (c) $\bar{u} = -1/2$, and (d) $\bar{u} = 1$. The phase portrait analysis shows that (27) is step convergent..

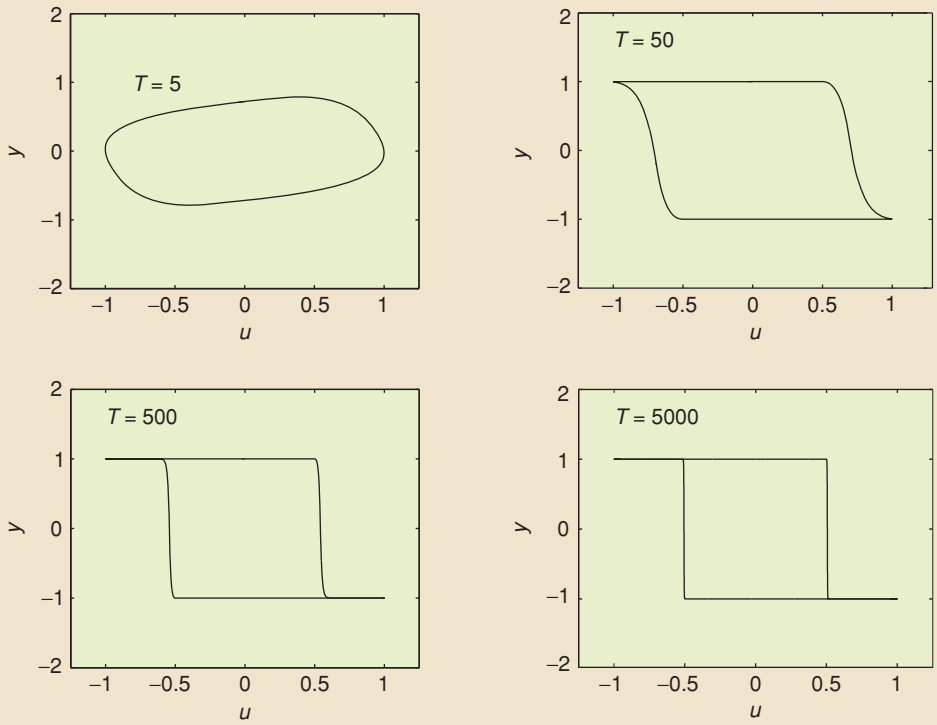

FIGURE 21 Hysteresis arising from the saturation nonlinearity. This periodic input-output map $\mathcal{H}(u_T, x_T(0))$ corresponds to (27) in Example 9 with $u_T(t) = \sin(2\pi/T)t$. Note that $\mathcal{H}(u_T, x_T(0))$ converges to a hysteretic map $\mathcal{H}_\infty(u, x_0)$.

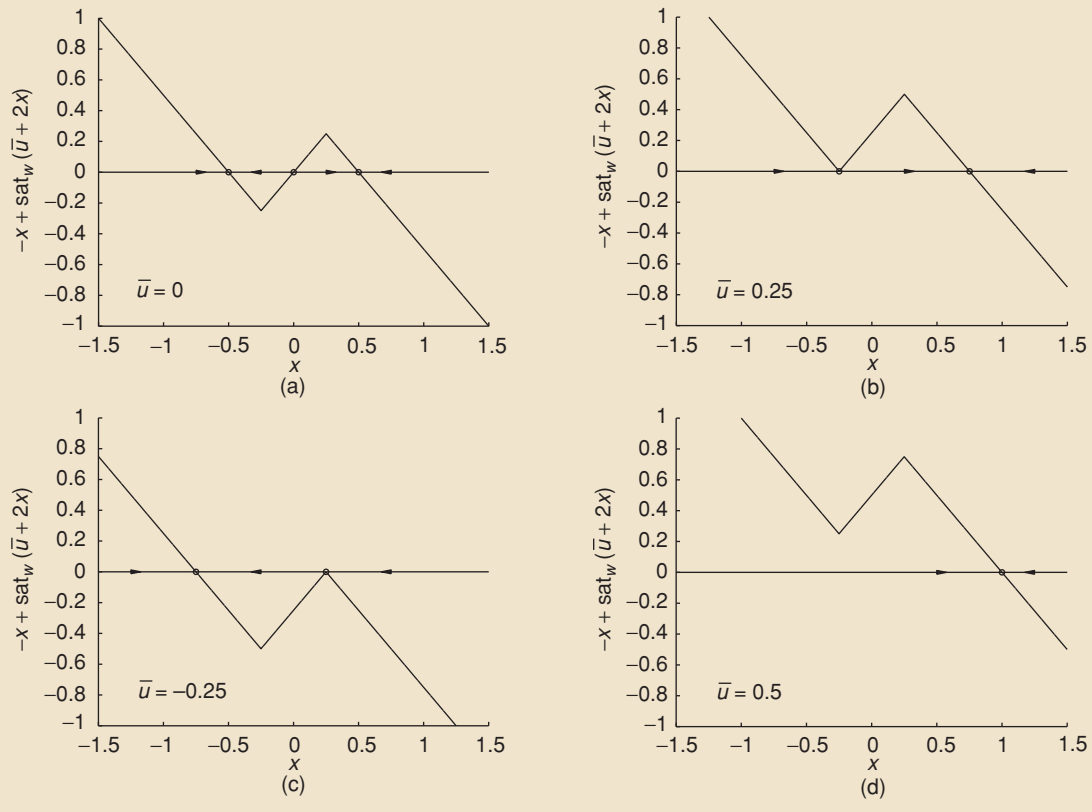

FIGURE 22 Plots of $x + \bar{u} - d_{2w}(2x)$ and the scalar phase portraits of (28) in Example 10, where (a) $\bar{u} = 0$, (b) $\bar{u} = 1/4$, (c) $\bar{u} = -1/4$, and (d) $\bar{u} = 1/2$. The phase portrait analysis shows that (28) is step convergent.

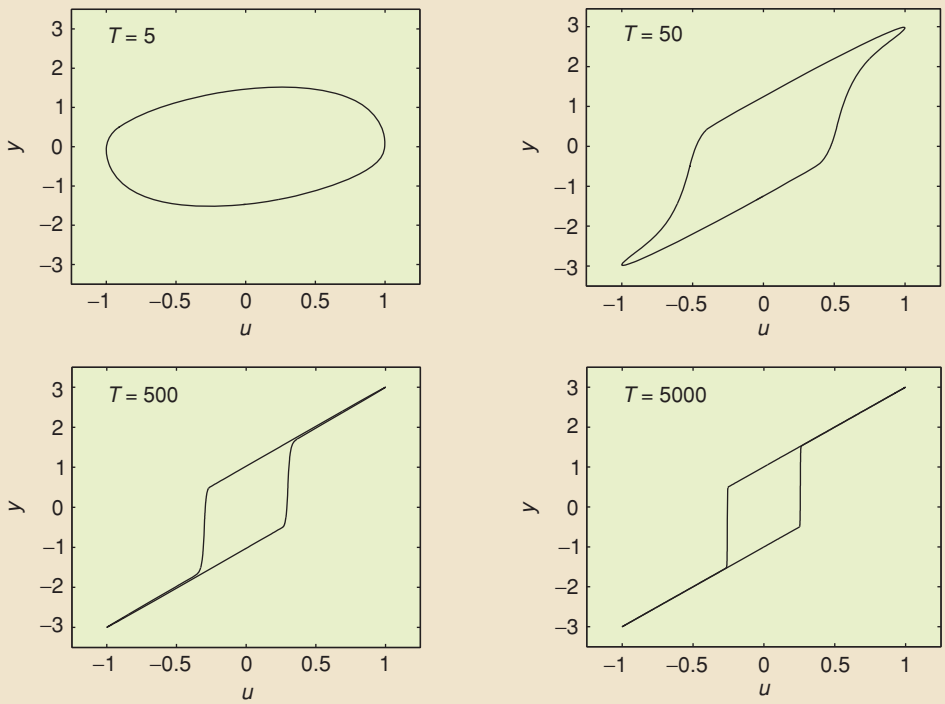

FIGURE 23 The periodic input-output map $\mathcal{H}(u_T, x_T(0))$ of (28) in Example 10 with $u_T(t) = \sin(2\pi/T)t$. Note that $\mathcal{H}(u_T, x_T(0))$ converges to a hysteretic map $\mathcal{H}_\infty(u, x_0)$.

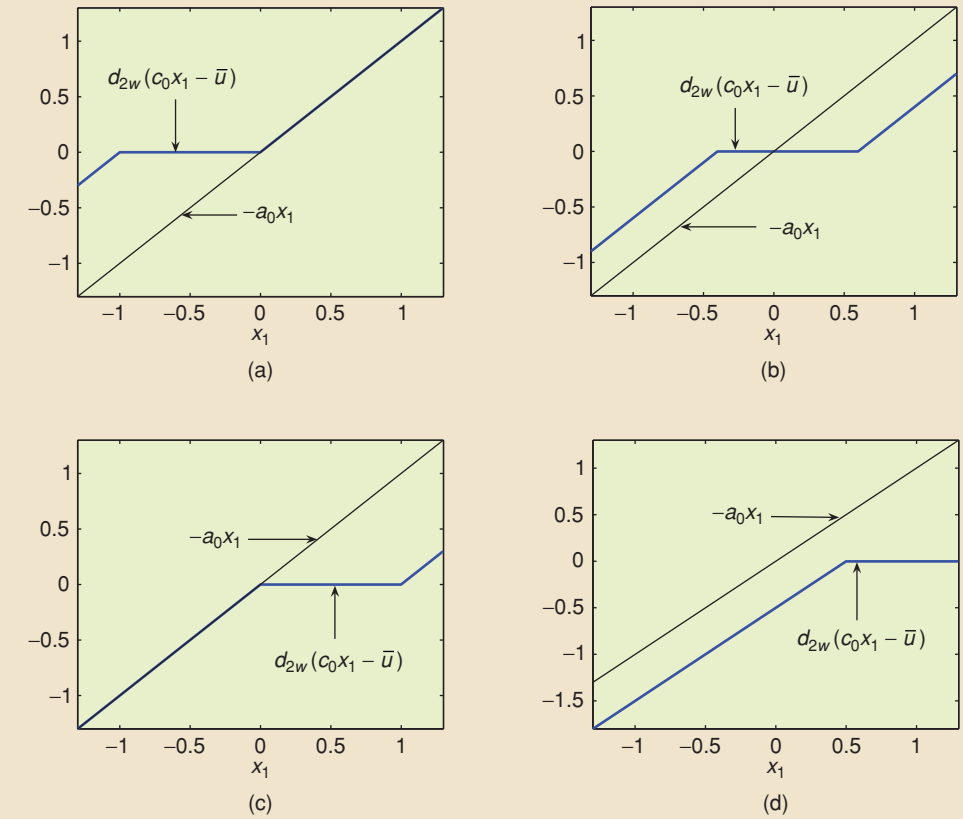

FIGURE 24 The four cases of solutions of (33) with $a_0 \neq 0$, and $a_0 + c_0 = 0$, and $c_0 > 0$. In (a) $\bar{u} = -w$ and the solutions of (33) form a set $\mathcal{X} = \{\bar{x} \in \mathbb{R} : \bar{x} \geq 0\}$; in (b) $|\bar{u}| < w$ and $\mathcal{X} = \{0\}$; and in (c) $\bar{u} = w$ and $\mathcal{X} = \{\bar{x} \in \mathbb{R} : \bar{x} \leq 0\}$. Finally, in (d) $|\bar{u}| > w$ and $\mathcal{X}$ is empty.

$\mathcal{X} = \{0\}$ for $|\bar{u}| < w$, a continuum of solutions $\mathcal{X} = \{\bar{x} \in \mathbb{R} : (\text{sign}\, c_0)\bar{x} \le 0\}$ for $\bar{u} = w$, and no solutions for $|\bar{u}| > w$. Hence $\mathcal{E}$ is given by

$$\mathcal{E} = \{(\bar{u}, \bar{y}) \in \mathbb{R}^2 : \bar{u} = w, \bar{y} \ge 0\} \cup \{(\bar{u}, \bar{y}) \in \mathbb{R}^2 : |\bar{u}| \le w, \bar{y} = 0\} \cup \{(\bar{u}, \bar{y}) \in \mathbb{R}^2 : \bar{u} = -w, \bar{y} \le 0\}. \quad (34)$$

Case 2

Let $a_0 = 0$. Then, as shown in Figure 25, for all values of $\bar{u}$ (33) has a continuum of solutions $\mathcal{X} = \{\bar{x} \in \mathbb{R} : (\bar{u} - w)/c_0 \le \bar{x} \le (\bar{u} + w)/c_0\}$ for $c_0 > 0$ and $\mathcal{X} = \{\bar{x} \in \mathbb{R} : (\bar{u} + w)/c_0 \le \bar{x} \le (\bar{u} - w)/c_0\}$ for $c_0 < 0$, for all $\bar{u} \in \mathbb{R}$. Hence, in both cases $\mathcal{E}$ is given by

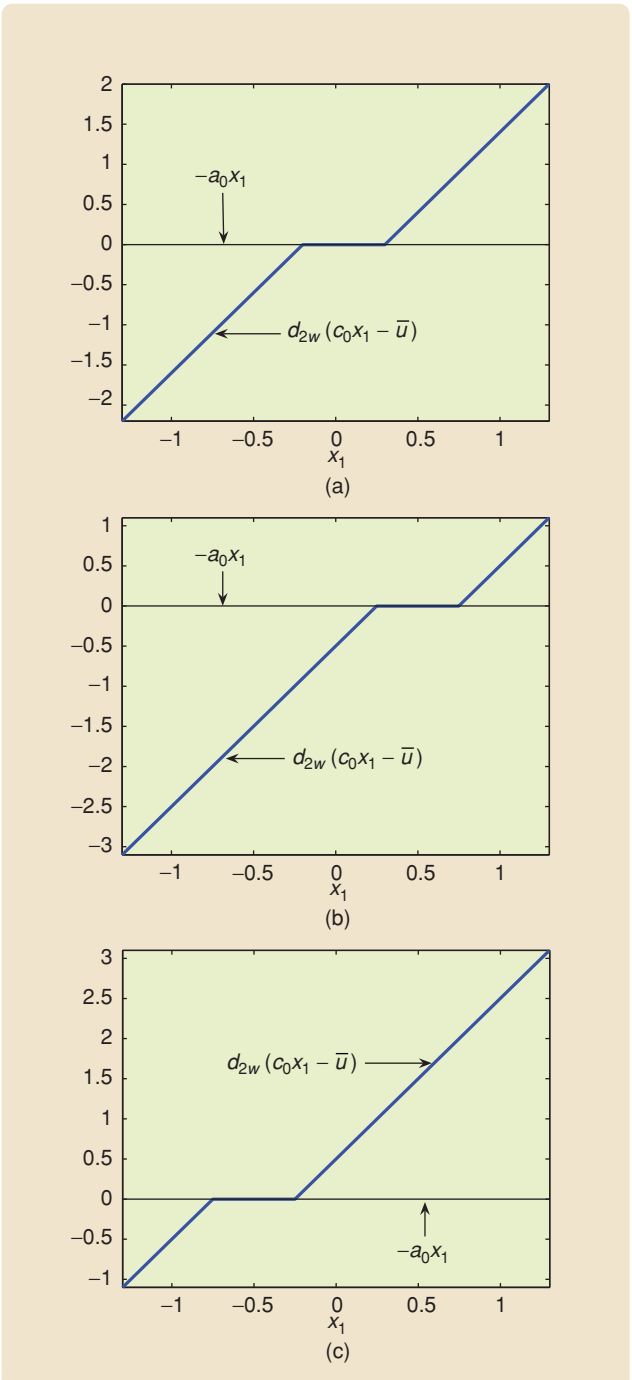

FIGURE 25 The solutions of (33) with $a_0 = 0$ and $c_0 > 0$. In (a) $|\bar{u}| < w$ and the solutions of (33) form a set $\mathcal{X} = \{\bar{x} \in \mathbb{R} : (\bar{u} - w)/c_0 \le \bar{x} \le (\bar{u} + w)/c_0\}$; in (b) $\bar{u} \ge w$ and $\mathcal{X}$ remains the same; and in (c) $\bar{u} \le -w$ and $\mathcal{X}$ remains the same.

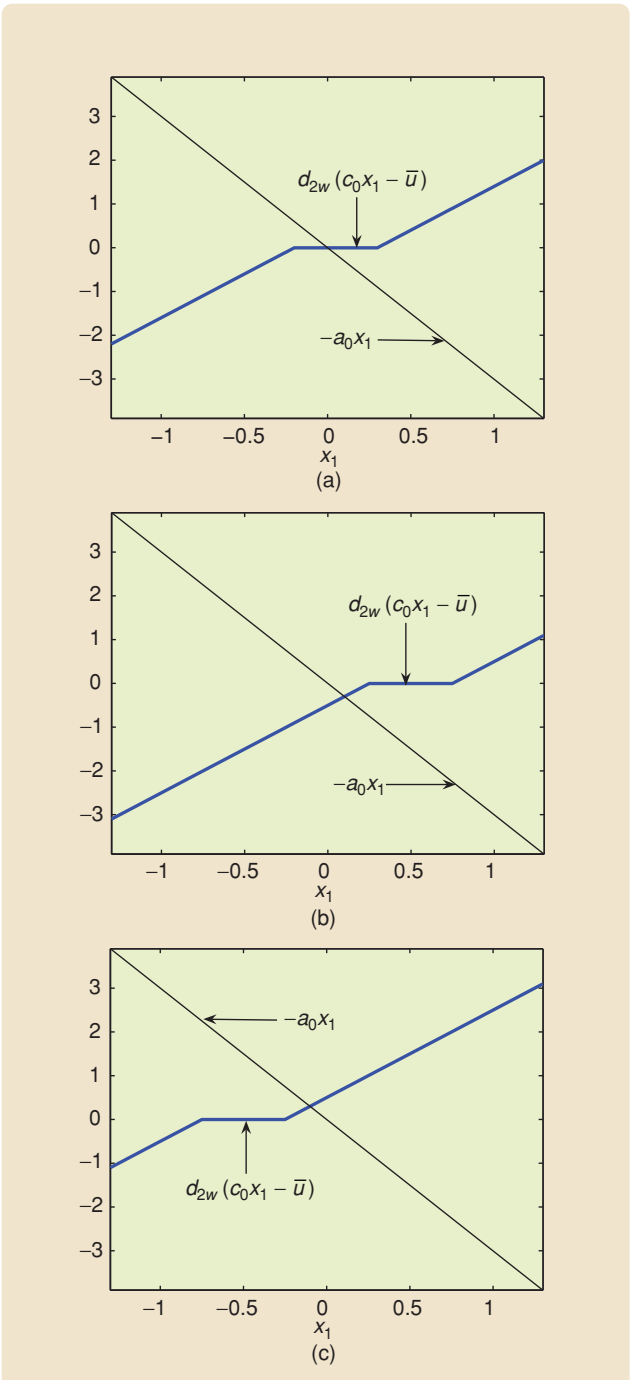

FIGURE 26 The solutions of (33) with $a_0 \neq 0$ and $a_0c_0 \ge 0$, or $a_0 \neq 0$ and $c_0(a_0 + c_0) < 0$. In (a) $|\bar{u}| < w$ and the solutions of (33) are unique $\mathcal{X} = \{1/(a_0 + c_0)d_{2w}(\bar{u})\}$; in (b) $\bar{u} \ge w$ and $\mathcal{X}$ remains the same; and in (c) $\bar{u} \le -w$ and $\mathcal{X}$ remains the same.

$$\mathcal{E} = \{(\bar{u}, \bar{y}) \in \mathbb{R}^2 : \bar{u} \in \mathbb{R}, \bar{u} - w \le \bar{y} \le \bar{u} + w\}. \tag{35}$$

Case 3

Let $a_0 \neq 0$ and $a_0 c_0 \geq 0$, or $a_0 \neq 0$ and $c_0(a_0 + c_0) < 0$. Then, as shown in Figure 26, (33) has a unique solution $\mathcal{X} = \{1/(a_0 + c_0) d_{2w}(\bar{u})\}$ for all $\bar{u} \in \mathbb{R}$. Hence $\mathcal{E}$ is given by

$$\mathcal{E} = \left\{(\bar{u}, \bar{y}) \in \mathbb{R}^2 : \bar{u} \in \mathbb{R}, \bar{y} = \frac{c_0}{a_0 + c_0} d_{2w}(\bar{u})\right\}. \tag{36}$$

Case 4

Let $a_0 \neq 0$ and $c_0(a_0 + c_0) > 0$. Then, as shown in Figure 27, (33) has nonunique solutions $\mathcal{X} = \{(\bar{u} - w)/(a_0 + c_0), 0, (\bar{u} + w)/(a_0 + c_0)\}$ for $|\bar{u}| < w$, two solutions $\mathcal{X} = \{0, (\bar{u} + w)/(a_0 + c_0)\}$ for $\bar{u} = w$, two solutions $\mathcal{X} = \{(\bar{u} - w)/(a_0 + c_0), 0\}$ for $\bar{u} = -w$, and a unique solution $\mathcal{X} = \{(\bar{u} + w)/(a_0 + c_0)\}$ for $\bar{u} > w$ and $\mathcal{X} = \{(\bar{u} - w)/(a_0 + c_0)\}$ for $\bar{u} < -w$. Hence $\mathcal{E}$ is given by

$$\begin{aligned}\mathcal{E} = &\left\{(\bar{u}, \bar{y}) \in \mathbb{R}^2 : \bar{u} < -w, \bar{y} = \frac{c_0(\bar{u} - w)}{a_0 + c_0}\right\} \\ &\cup \left\{(\bar{u}, \bar{y}) \in \mathbb{R}^2 : |\bar{u}| \le w, \bar{y} = \frac{c_0(\bar{u} - w)}{a_0 + c_0}, \ 0, \ \frac{c_0(\bar{u} + w)}{a_0 + c_0}\right\} \\ &\cup \left\{(\bar{u}, \bar{y}) \in \mathbb{R}^2 : \bar{u} > w, \bar{y} = \frac{c_0(\bar{u} + w)}{a_0 + c_0}\right\}. \end{aligned} \tag{37}$$

Note that, if $a_0 + c_0 = 0$, then, for each constant input $\bar{u}$ such that $|\bar{u}| > w$, (29), (30) does not have an equilibrium, and thus system is not step convergent. Now, assume that (29), (30) is step convergent. Then $\mathcal{E}$ is given by either (35), (36), or (37). Suppose $a_0 = 0$ (case 2) and thus $\mathcal{E}$ is given by (35). Then $\mathcal{E}$ is a multivalued map as shown in Figure 28(b). Therefore, $\mathcal{H}_\infty(u, x_0)$ is hysteretic as shown in Figure 29(a). Now, suppose $a_0 \neq 0$ and $a_0 c_0 \geq 0$, or $a_0 \neq 0$ and $c_0(a_0 + c_0) < 0$ (case 3) and thus $\mathcal{E}$ is given by (36). Then $\mathcal{E}$ is a single-valued map as shown in Figure 28(c). Therefore, $\mathcal{H}_\infty(u, x_0)$ is not hysteretic as shown in Figure 29(b). Finally, suppose $a_0 \neq 0$ and $c_0(a_0 + c_0) > 0$ (case 4), and thus $\mathcal{E}$ is given by (37). Then $\mathcal{E}$ is a single-valued map for $|\bar{u}| < w$ and is a multivalued map for $|\bar{u}| > w$ as shown in Figure 28(d). Therefore, $\mathcal{H}_\infty(u, x_0)$ is hysteretic when $\max_{t \ge 0} u(t) \geq w$ and $\min_{t \ge 0} u(t) \leq -w$ as shown in Figure 29(c). Table 1 summarizes the characteristics of $\mathcal{H}_\infty(u, x_0)$ in all of the cases.

Example 11

Consider (29), (30) with

$$A = \begin{bmatrix} 0 & 1 \\ -1 & -2 \end{bmatrix}, \quad B = \begin{bmatrix} 0 \\ 1 \end{bmatrix}, \quad C = \begin{bmatrix} 1 & 2 \end{bmatrix},$$

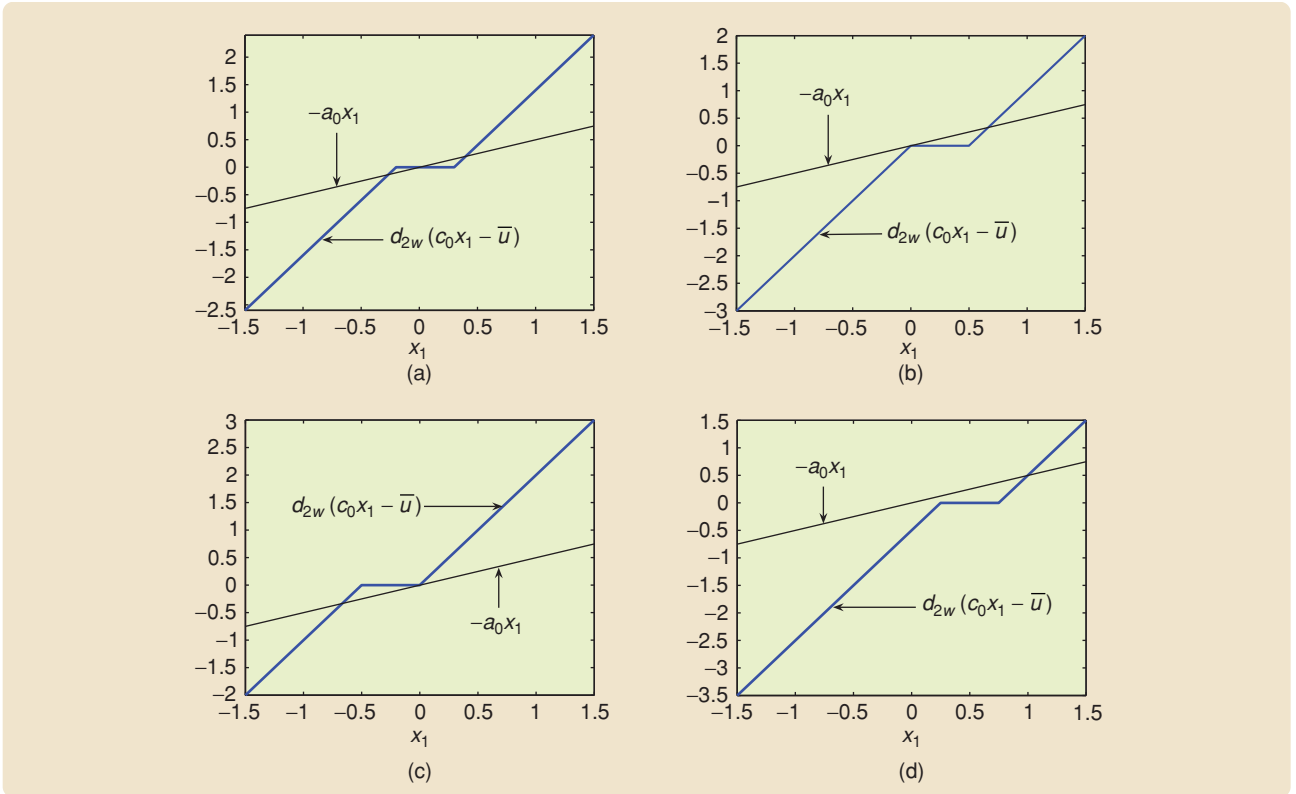

FIGURE 27 The four cases of solutions of (33) with $a_0 \neq 0$ and $c_0(a_0 + c_0) > 0$. In (a) $|\bar{u}| \leq w$ and (33) has three solutions $\mathcal{X} = \{(\bar{u} - w)/(a_0 + c_0), 0, (\bar{u} + w)/(a_0 + c_0)\}$; in (b) $\bar{u} = w$ and (33) has two solutions $\mathcal{X} = \{0, (\bar{u} + w)/(a_0 + c_0)\}$; and in (c) $\bar{u} = -w$ and (33) has two solutions $\mathcal{X} = \{(\bar{u} - w)/(a_0 + c_0), 0\}$. Finally, in (d) $|\bar{u}| > w$, and (33) has a unique solution $\mathcal{X} = \{(\bar{u} - w)/(a_0 + c_0)\}$ if $\bar{u} < -w$ or $\mathcal{X} = \{(\bar{u} + w)/(a_0 + c_0)\}$ if $\bar{u} > w$.

TABLE 1 The characteristic of $\mathcal{H}_\infty(u, x_0)$ of the deadzone-based backlash hysteresis model in various cases. The limiting periodic input-output map $\mathcal{H}_\infty(u, x_0)$ exists in four distinct cases, which depend on the values of a_0 and c_0.

Case 1	$a_0 \neq 0$ and $a_0 + c_0 = 0$	Not hysteretic
Case 2	$a_0 = 0$	Hysteretic (traversal type)
Case 3	$a_0 \neq 0$ and $a_0 c_0 \geq 0$, or $a_0 \neq 0$ and $c_0(a_0 + c_0) < 0$	Not hysteretic
Case 4	$a_0 \neq 0$ and $c_0(a_0 + c_0) > 0$	Hysteretic (bifurcation type) if $\max_{t\geq 0} u(t) \geq w$ and $\min_{t\geq 0} u(t) \leq -w$.

and $w = 0.5$. Since $a_0 = 1 \neq 0$ and $a_0 c_0 = 1 \geq 0$, the model satisfies case 3, and $\mathcal{H}_\infty(u, x_0)$ is not hysteretic from Table 1. Figure 30 shows that $\mathcal{H}(u_T, x_T(0))$ converges to a single-valued map.

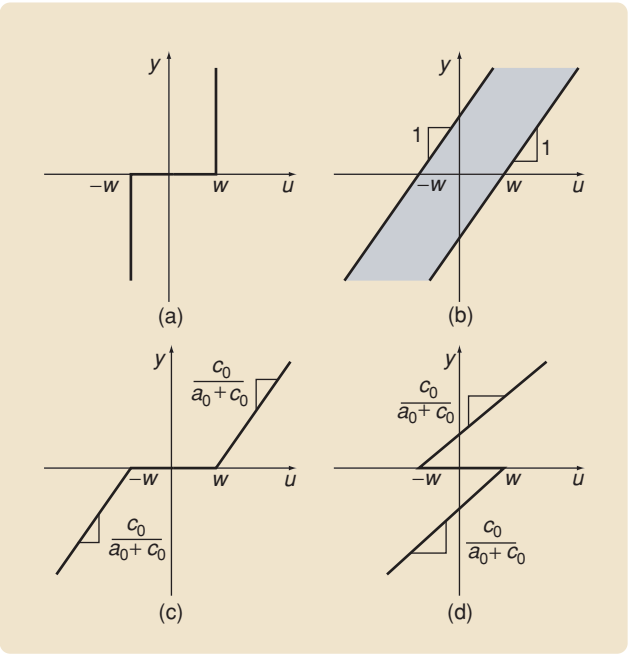

FIGURE 28 The input-output equilibria map $\mathcal{E}$ of (a) case 1 given by (34), (b) case 2 given by (35), (c) case 3 given by (36), and (d) case 4 given by (37). The shape of the input-output equilibria map $\mathcal{E}$ determines whether the system is hysteretic or not.

Example 12

Reconsider (29), (30) with

$$A = \begin{bmatrix} 0 & 1 \\ 1 & -2 \end{bmatrix}, \quad B = \begin{bmatrix} 0 \\ 1 \end{bmatrix}, \quad C = \begin{bmatrix} 2 & 0 \end{bmatrix}, \tag{38}$$

and $w = 0.5$. Since $a_0 = -1 \neq 0$ and $c_0(a_0 + c_0) = 2 > 0$, the model is case 4, and $\mathcal{H}_\infty(u, x_0)$ is hysteretic from Table 1. Figure 31 shows that $\mathcal{H}(u_T, x_T(0))$ converges to a hysteretic map.

A MULTILOOP NONLINEAR FEEDBACK EXAMPLE

The monotone system

$$\dot{x}_1(t) = \frac{\alpha_1}{1 + (u(t)x_2(t))^{\beta_1}} - x_1(t), \tag{39}$$

$$\dot{x}_2(t) = \frac{\alpha_2}{1 + x_1^{\beta_2}(t)} - x_2(t), \tag{40}$$

$$y(t) = x_2(t), \tag{41}$$

where α_1, α_2, β_1, and β_2 are positive constants, is commonly encountered in biology and, in the given form, represents a model of gene expression [10]. As illustrated by Figure 32, (39)–(41) is a single-input, single-output system with the feedback nonlinearities

$$\phi_i(z) = \frac{\alpha_i}{1 + z^{\beta_i}}, \qquad i = 1, 2. \tag{42}$$

Notice that when $\phi_2 = 0$, (39)–(41) is identical to (5) and (6) (see Figure 1) with $\phi = \phi_1$, and

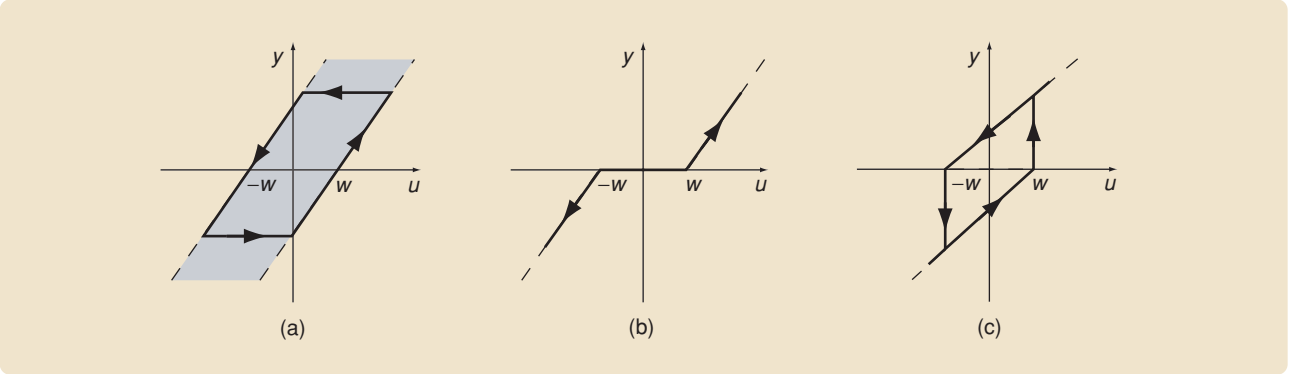

FIGURE 29 The limiting periodic input-output map $\mathcal{H}_\infty(u, x_0)$ (solid) and the input-output equilibria set $\mathcal{E}$ (dashed) of (a) case 2, (b) case 3, and (c) case 4 of Figure 28. The input-output maps in (a) and (c) are hysteretic, whereas the map in (b) is not. Furthermore, the hysteretic map in (a) is traversal type, whereas the hysteretic map in (b) is bifurcation type.

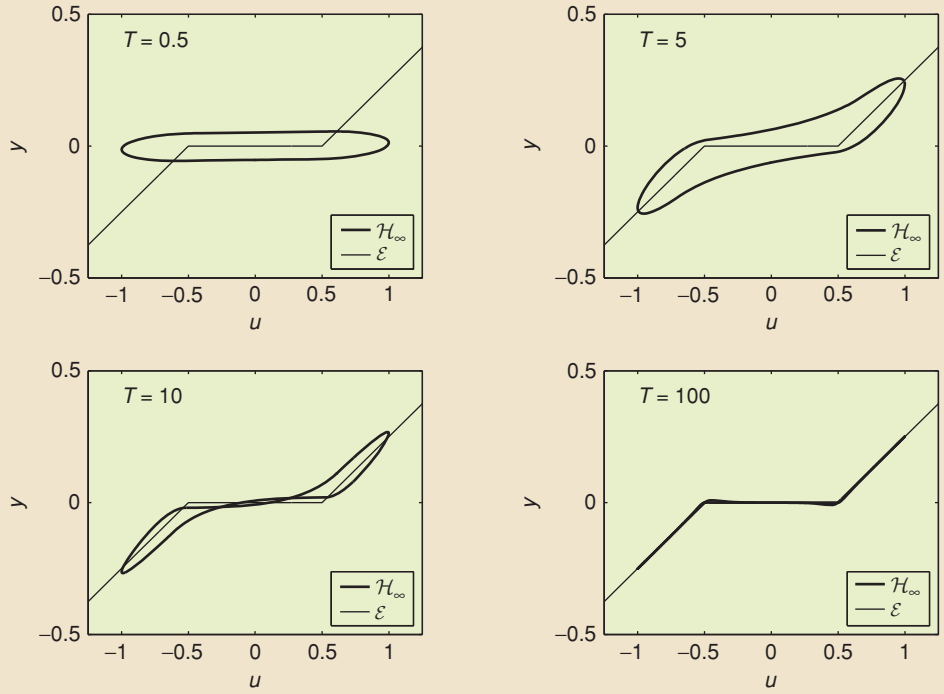

FIGURE 30 Periodic input-output map $\mathcal{H}(u_T, x_T(0))$ and input-output equilibria map $\mathcal{E}$ of Example 11 with $u(t) = \sin(2\pi/T)t$. Note that this model is case 3 and is not hysteretic.

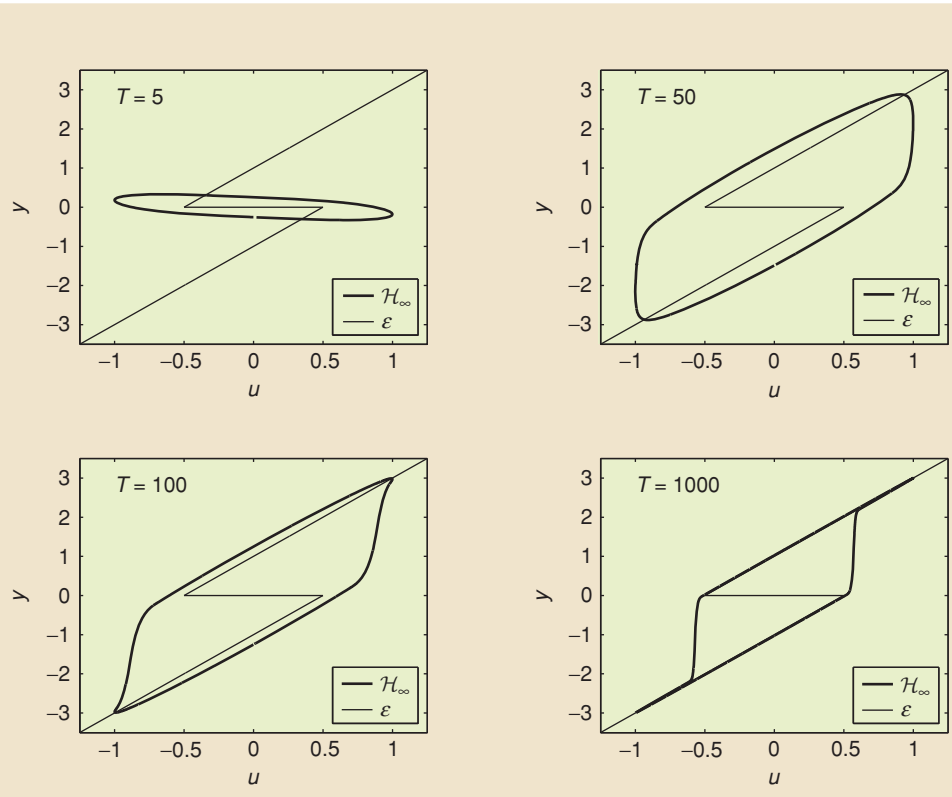

FIGURE 31 $\mathcal{H}(u_T, x_T(0))$ and $\mathcal{E}$ of Example 12 with $u(t) = \sin(2\pi/T)t$. Note that this model is case 4 and $\mathcal{H}(u_T, x_T(0))$ converges to a hysteretic map $\mathcal{H}_\infty(u, x_0)$.

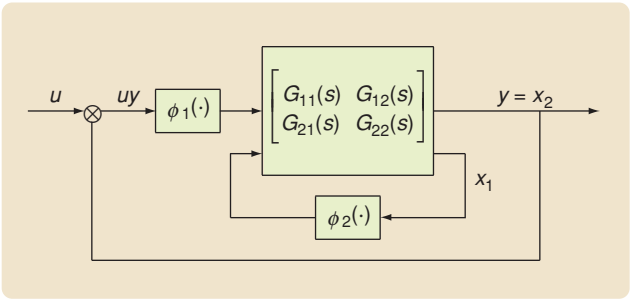

FIGURE 32 Block diagram of the single-input, single output system of (39)–(41). Notice that the system is identical to that in Figure 1 when the nonlinearity $\phi_2 = 0$.

$$\begin{bmatrix} G_{11}(s) & G_{12}(s) \\ G_{21}(s) & G_{22}(s) \end{bmatrix} = \begin{bmatrix} 0 & G(s) \\ G(s) & 0 \end{bmatrix}. \tag{43}$$

The input-output equilibria map $\mathcal{E}$ of (39)–(41) is shown in Figure 33 with $\alpha_1 = 1.3$, $\alpha_2 = 1.3$, $\beta_1 = 3$, and $\beta_2 = 6$. As can be seen by comparing Figure 33 with Figure 4, the shape of $\mathcal{E}$ for (39)–(41) is similar to the shape of $\mathcal{E}$ for the cubic hysteresis model in Example 4.

For each constant input $u(t) = \bar{u}$, (39)–(41) have one, two, or three equilibria, depending on the value of $\bar{u}$. The limiting values of $\bar{u}$ for which the system transitions from three to two equilibria are $\bar{u}_1 \approx 0.8$ and $\bar{u}_2 \approx 1.35$. As shown in Figure 34(a), for $\bar{u}_1 < \bar{u} < \bar{u}_2$ the system has three equilibria, of which two are stable and one is unstable. For $\bar{u} = \bar{u}_1$ or $\bar{u} = \bar{u}_2$ the system has two stable equilibria, as shown in Figure 34(b) and (c), respectively. For $\bar{u} < \bar{u}_1$ or $\bar{u} > \bar{u}_2$ the system has only one equilibrium as shown in Figure 34(d).

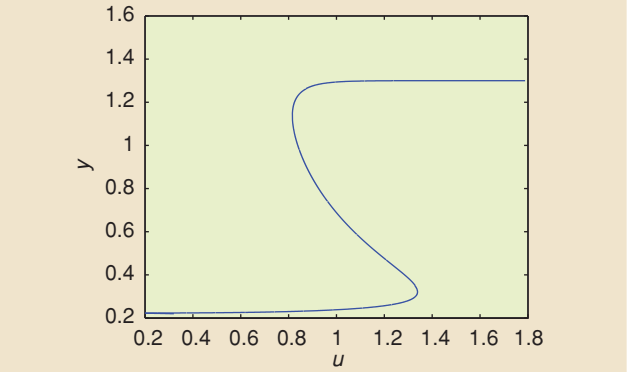

FIGURE 33 The input-output equilibria map $\mathcal{E}$ of (39)–(41) with $\alpha_1 = 1.3$, $\alpha_2 = 1.3$, $\beta_1 = 3$, and $\beta_2 = 6$. Notice that the shape of $\mathcal{E}$ given by (39)–(41) is similar to the shape of $\mathcal{E}$ given by the cubic hysteresis model in Example 4.

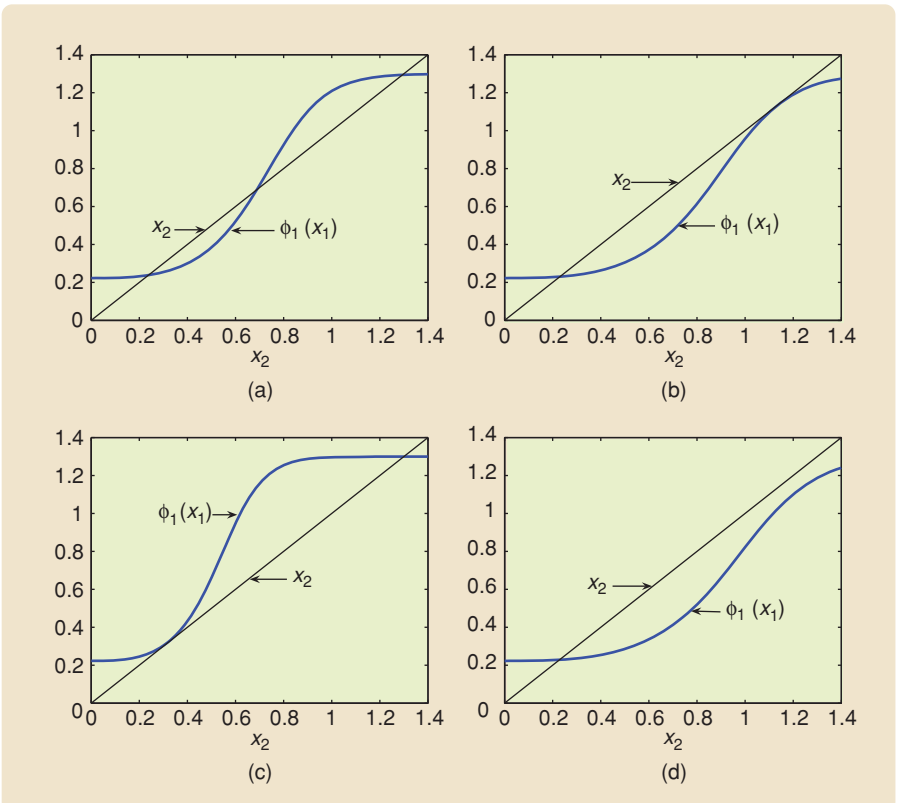

FIGURE 34 The number of equilibrium points of (39)–(41) as a function of $\bar{u}$. For $\bar{u}_1 \approx 0.8$ and $\bar{u}_2 \approx 1.35$, if $\bar{u}_1 < \bar{u} < \bar{u}_2$, then (39)–(41) have three equilibria, two stable and one unstable as shown in (a). For $\bar{u} = \bar{u}_1$ and $\bar{u} = \bar{u}_2$ the system has two equilibria as shown in (b) and (c), respectively. For $\bar{u} < \bar{u}_1$ or $\bar{u} > \bar{u}_2$ the system has only one equilibrium state as shown in (d).

The periodic input-output map $\mathcal{H}(u_T, x_T(0))$ of (39)–(41) with $u_T(t) = 2|\sin(2\pi/T)t|$ is shown in Figure 35. As $T \to \infty$, $\mathcal{H}(u_T, x_T(0))$ converges to a hysteretic map $\mathcal{H}_\infty(u, x_0)$. Notice that the $\mathcal{H}_\infty(u, x_0)$ of (39)–(41) resembles $\mathcal{H}_\infty(u, x_0)$ of the cubic hysteresis model in Example 4, as expected based on the shape of the input-output equilibria map $\mathcal{E}$.

CONCLUSION

In this article we considered nonlinear feedback models for hysteresis. The relationship between step convergence and the hysteresis map of the model was investigated. The class of models that exhibit hysteresis was determined, and the shape of the hysteresis maps was related to the limiting equilibria set. Numerical examples illustrate the analysis.

ACKNOWLEDGMENTS

This research was supported in part by the National Science Foundation under grant ECS–0225799.

REFERENCES

[1] M.A. Krasnosel'skiĭ and A.V. Pokrovskiĭ, *Systems with Hysteresis*. New York: Springer-Verlag, 1980.

[2] J.W. Macki, P. Nistri, and P. Zecca, "Mathematical models for hysteresis," *SIAM Rev.*, vol. 35, no. 1, pp. 94–123, 1993.

[3] I.D. Mayergoyz, *Mathematical Models of Hysteresis*. New York: Springer-Verlag, 1991.

[4] A. Visintin, *Differential Models of Hysteresis*. New York: Springer-Verlag, 1994.

[5] D.S. Bernstein, "Ivory ghost," *IEEE Control Syst. Mag.*, vol. 27, pp. 16–17, 2007.

[6] J.B. Collings and D.J. Wollkind, "Metastability, hysteresis and outbreaks in a temperature-dependent model for a mite predator-prey interaction," *Math. Comp. Modelling*, vol. 13, pp. 91–103, 1990.

[7] D.N. Maywar, G.P. Agrawal, and Y. Nakano, "All-optical hysteresis control by means of cross-phase modulation in semiconductor optical amplifiers," *J. Opt. Soc. Amer. B*, vol. 18, no. 7, pp. 1003–1013, 2001.

[8] G. Cao and P.P. Banerjee, "Theory of hysteresis and bistability during transmission through a linear nondispersive-nonlinear dispersive interface," *J. Opt. Soc. Amer. B*, vol. 6, no. 2, pp. 191–198, 1989.

[9] N.F. Mitchell, J. O'Gorman, J. Hegarty, and J.C. Connoly, "Optical bistability and X-shaped hysteresis in laser diode amplifiers," in *Lasers and Electro-Optics Society Annual Meeting*, 1993, pp. 520–521.

[10] D. Angeli and E.D. Sontag, "Multi-stability in monotone input/output systems," *Syst. Contr. Lett.*, vol. 51, pp. 185–202, 2004.

[11] L.O. Chua and S.C. Bass, "A generalized hysteresis model," *IEEE Trans. Circuit Theory*, vol. 19, no. 1, pp. 36–48, 1972.

[12] J. Oh and D.S. Bernstein, "Semilinear Duhem model for rate-independent and rate-dependent hysteresis," *IEEE Trans. Automat. Contr.*, vol. 50, no. 5, pp. 631–645, 2005.

[13] A.K. Padthe, B. Drincic, J. Oh, D.D. Rizos, S.D. Fassois, and D.S. Bernstein, "Duhem modeling of friction-induced hysteresis: Experimental determination of gearbox stiction," *IEEE Control Syst. Mag.*, vol. 28, pp. 90–107, 2008.

[14] M. Nordin and P. Gutman, "Controlling mechanical systems with backlash—a survey," *Automatica*, vol. 38, no. 10, pp. 1633–1649, 2002.

[15] M. Nordin, J. Galic, and P. Gutman, "New models for backlash and gear play," *Int. J. Adaptive Contr. Signal Processing*, vol. 11, pp. 49–63, 1997.

[16] G. Tao and P.V. Kokotović, *Adaptive Control of Systems with Actuator and Sensor Nonlinearities*. New York: Wiley, 1996.

[17] C. Su, Y. Stepanenko, J. Svoboda, and T.P. Leung, "Robust adaptive control of a class of nonlinear systems with unknown backlash-like hysteresis," *IEEE Trans. Automat. Contr.*, vol. 45, no. 12, pp. 2427–2432, 2000.

[18] M.P. Mortell, R.E. O'Malley, A. Pokrovskii, and V. Sobolev, *Singular Perturbations and Hysteresis*. Philadelphia, PA: SIAM, 2001.

[19] F. Scheibe and M.C. Smith, "A behavioural view of play in mechanical networks," in *Proc. European Control Conf.*, 2007, pp. 3755–3762.

[20] J. Guckenheimer and P. Holmes, *Nonlinear Oscilllations, Dynamical Systems, and Bifurcations of Vector Fields*. New York: Springer-Verlag, 1983.

[21] D.S. Bernstein and S.P. Bhat, "Lyapunov stability, semistability, and asymptotic stability of matrix second-order systems," *ASME Trans. J. Vibr. Acoustics*, vol. 117, pp. 145–153, 1995.

[22] S.P. Bhat and D.S. Bernstein, "Nontangency-based Lyapunov tests for convergence and stability in systems having a continuum of equilibria," *SIAM J. Contr. Optim.*, vol. 42, pp. 1745–1775, 2003.

[23] J.K. Hale and H. Koçak, *Dynamics and Bifurcations*. New York: Springer-Verlag, 1991.

[24] S.L. Lacy, D.S. Bernstein, and S.P. Bhat, "Hysteretic systems and step-convergent semistability," in *Proc. American Control Conf.*, Chicago, IL, June 2000, pp. 4139–4143.

[25] J. Oh and D.S. Bernstein, "Step convergence analysis of nonlinear feedback hysteresis models," in *Proc. American Control Conf.*, Portland, OR, 2005, pp. 697–702.

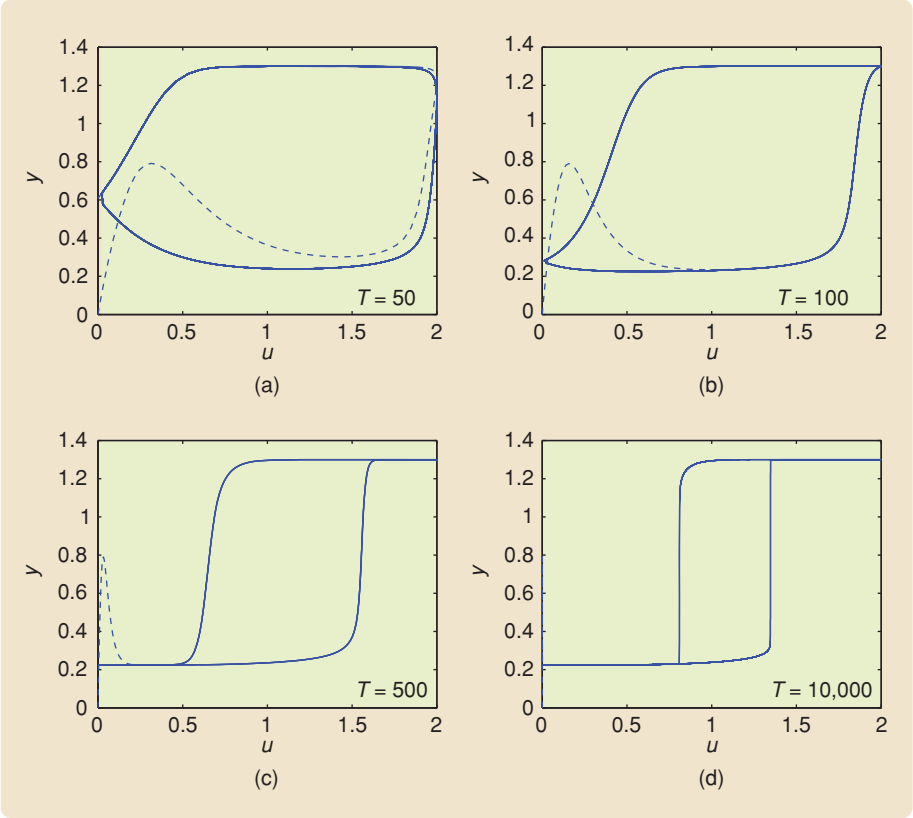

FIGURE 35 The periodic input-output map $\mathcal{H}(u_T, x_T(0))$ corresponding to (39)–(41) with $u_T(t) = 2|\sin(2\pi/T)t|$. Note that $\mathcal{H}(u_T, x_T(0))$ converges to a hysteretic map $\mathcal{H}_\infty(u, x_0)$ as $T \to \infty$.

AUTHOR INFORMATION

JinHyoung Oh received the bachelor's degree in control and instrumentation engineering from Korea University and the master's degrees in aerospace engineering and applied mathematics from Georgia Institute of Technology. He received the Ph.D. degree in aerospace engineering from the University of Michigan in 2005. He is currently employed by AutoLiv as a research engineer.

Bojana Drincic (bojanad@umich.edu) received her bachelor's degree in aerospace engineering from the University of Texas at Austin in 2007. She is now pursuing a Ph.D. at the University of Michigan. Her research interests include hysteretic systems, systems with friction, and spacecraft dynamics and control. She can be contacted at the Aerospace Engineering Department, University of Michigan, 1320 Beal Ave., Ann Arbor, MI 48109 USA.

Dennis S. Bernstein is a professor in the Aerospace Engineering Department at the University of Michigan. He is editor-in-chief of *IEEE Control Systems Magazine* and the author of *Matrix Mathematics* (Princeton University Press). His interests are in system identification and adaptive control for aerospace applications.